Chem Catalysis

CellPress

Resource

Site-directed spin labeling-electron paramagnetic resonance spectroscopy in biocatalysis: Enzyme orientation and dynamics in nanoscale confinement

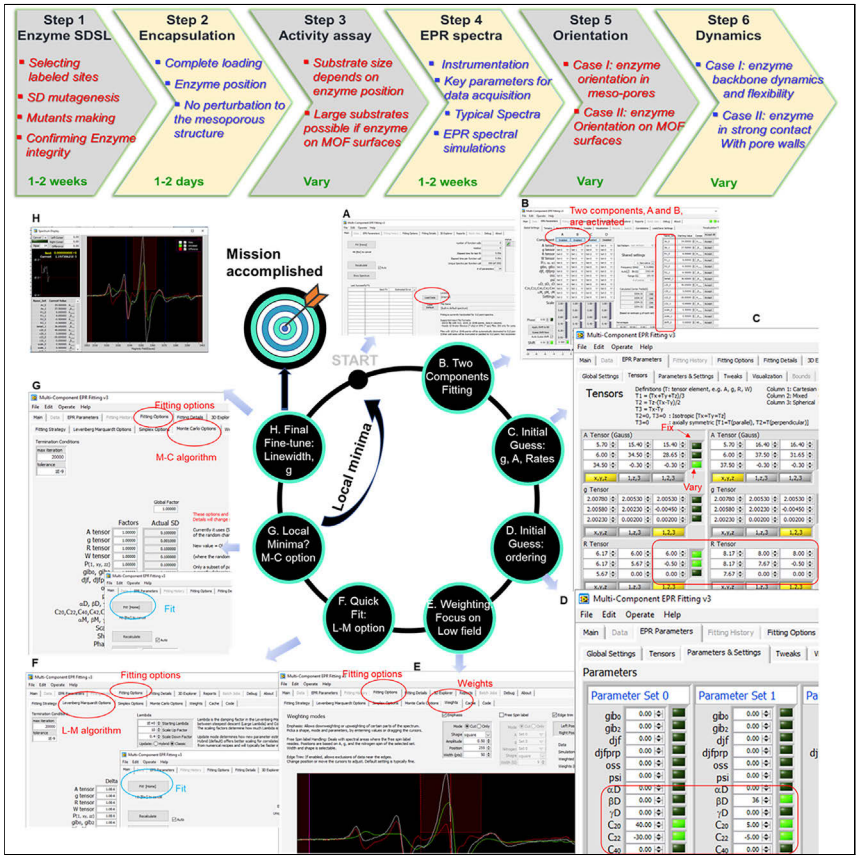

In this resource article, Yang and colleagues introduce a general procedure that can reveal the orientation and backbone dynamics of enzymes entrapped in mesoporous materials based on metal-organic materials (MOMs) by using X-band SDSL-EPR. They demonstrate the method by using recently published works focusing on enzyme-MOM interfaces, as well as highlight cautions and potential solutions at each step. They then summarize a variety of other EPR techniques and spin labels in order to pinpoint their potential applications in heterogeneous biocatalysis in the near future.

Yanxiong Pan, Hui Li, Qiaobin Li, Mary Lenertz, Xiao Zhu, Bingcan Chen, Zhongyu Yang

zhongyu.yang@ndsu.edu

Highlights

Enzyme orientation is determined by using EPR to probe its contact with nanoscale pores

Enzyme dynamics in nanoscale pores and associated catalytic activities are revealed

Protocols and procedures are given for experimental data acquisition, analysis, and interpretation

Various EPR techniques and spin labels can be extended to heterogeneous biocatalysis

Pan et al., Chem Catalysis 1, 207–231
June 17, 2021
https://doi.org/10.1016/j.checat.2021.03.005

Chem Catalysis

CellPress

Resource

Site-directed spin labeling-electron paramagnetic resonance spectroscopy in biocatalysis: Enzyme orientation and dynamics in nanoscale confinement

Yanxiong Pan,[1] Hui Li,[2] Qiaobin Li,[1] Mary Lenertz,[1] Xiao Zhu,[3,4] Bingcan Chen,[2] and Zhongyu Yang[1,5,*]

SUMMARY

Site-directed spin labeling (SDSL) in combination with electron paramagnetic resonance (EPR) spectroscopy probes the otherwise inaccessible structural information in complex biological systems. We recently extended SDSL-EPR to reveal the relative orientation and backbone dynamics of enzymes upon encapsulation in mesoporous nanostructures, which set the structural basis underlying the observed biocatalytic activity. Our strategy had generated interest in the biocatalysis community, and thus in this resource article, we contribute an introduction to the principles and experimental procedure that generalize SDSL-EPR to heterogeneous biocatalysis. We will focus on enzymes in mesoporous materials with examples demonstrating the methods and cautions of potential pitfalls. The ultimate goal is to provide the biocatalysis community with a powerful resource to fill in a long-standing knowledge gap in heterogeneous biocatalysis and the structure-function relationship of enzymes at the interface of enzyme-mesoporous materials and utilize the structural insights to guide the rational design of porous platforms for enzyme immobilization.

INTRODUCTION

Enzymes are among the most critical players in biocatalysis because of their high specificity, selectivity, and biocompatibility, yet their high cost is a major hurdle limiting their broader applications. Heterogeneous biocatalysis based on enzyme immobilization can improve the reusability and recyclability and thus the cost efficiency.[1–5] However, most immobilization approaches rely on chemical linking or physical adsorption, which faces chemical perturbation or leaching, respectively.[6,7] Encapsulation of enzymes into porous materials is an alternative that offers enhanced cost efficiency, reduced leaching, and enzyme protection against harsh environments, although the substrate size is often limited.[8–10] Unique platforms for enzyme immobilization are metal-organic frameworks (MOFs) and covalent-organic frameworks (COFs), wherein enzymes can be loaded via diffusion or co-precipitation,[11–19] the latter of which even allows for large-substrate biocatalysis.[20–23] Therefore, MOFs and COFs are by far the most optimal platforms, offering desirable substrate selectivity and diffusivity and even enhanced catalytic efficiency in certain cases.

Despite the exciting developments in enzyme-MOF and -COF research, a fundamental knowledge gap has remained elusive: how does nanoscale confinement influence enzyme performance, and what is the underlying structural basis?[24] Answering these questions will not only improve our understanding of the structure-function relationship of enzymes but also guide the rational design of porous materials with desirable

The bigger picture

Enzyme immobilization in nanoscale confinement offers enhanced enzyme protection and reusability, yet the structure-function relationship of the entrapped enzymes remains elusive. Site-directed spin labeling in combination with electron paramagnetic resonance (EPR) spectroscopy has primarily been applied in determining protein structural information in complex biological systems. In this resource article, we introduce the extension of the X-band continuous-wave EPR with a methanethiosulfonate spin label to reveal enzyme structural basis upon immobilization into nanoscale confinement. Using our recent works as examples, we demonstrate the method for determining enzyme orientation and backbone dynamics upon immobilization with a special focus on generalizing the method to heterogeneous biocatalysis and cautions in each step. Furthermore, we summarize the recent findings in other EPR techniques and spin labels so that the whole EPR toolbox can be extended to heterogeneous biocatalysis.

functionality for enzyme immobilization. In a heterogeneous biocatalysis system, the most important structural information is the conformational dynamics and relative orientation of the enzyme with respect to the surfaces of the materials, which are related to substrate recognition and binding as well as protein function. Determining this information in a mesoporous material, however, is a challenging task for "surface"-based techniques because the enzymes are "covered" by the pore walls. The dynamics and heterogeneity in conformation limit crystallographic approaches, and the slow motion challenges the NMR-based structural determination. Adding a "spy" or "probe" to the enzyme seems promising,[25,26] yet most fluorophores are large in size and can interfere with enzyme function or block enzyme loading.

Site-directed spin labeling in combination with electron paramagnetic resonance (SDSL-EPR) could overcome these barriers. The EPR "spy," often known as a spin label, is usually the size of a lysine, creating negligible perturbation to the host protein.[27] The most widely used EPR label, a methanethiosulfonate nitroxide, can be conveniently attached to the protein thiols (i.e., cysteine) via disulfide bonds. By creating cysteine mutations at the sites of interest via site-directed mutagenesis, EPR spin labels can, in principle, be placed at any site of interest. For cysteine-rich proteins, other labeling strategies are available.[28,29] Once labeled, at room temperature, the protein dynamics at the labeled site can be probed by the penetrating power of microwave radiation regardless of the heterogeneity and complexity of the sample[30–33] as long as the water volume in the sample is sufficiently small (to avoid microwave absorption by water).[34,35] With two probes attached, the distance distribution between the labels can be determined as well.[36–38] Thus, SDSL-EPR is an advantageous approach to probing the structural information of enzymes in complex systems, including heterogeneous biocatalysis.

Thus far, SDSL-EPR has mainly been applied in transmembrane proteins, protein-DNA and protein-protein complexes, and proteins in real cells.[39–60] Typical structural information obtained includes the large-scale domain motion of proteins upon substrate or partner binding, orientation and relative arrangement of helices in membranes, and local polarity and environments. There has been limited effort in applying SDSL-EPR to the interface of enzymes and mesoporous materials, especially MOFs and COFs, yet this effort can reveal the interplay of enzyme orientation, dynamics, and activity at these interfaces. Recently, our group has shown the potential of such extension[20–22,61,62] (see Pan et al.[61] in this issue of *Chem Catalysis*), which has generated interest in the community. Thus, through this resource article, we summarize the procedure and practical aspects of using SDSL-EPR to reveal key structural information of enzymes in mesoporous MOFs and COFs. The ultimate goal is to provide a resource that can be generalized to other heterogeneous biocatalysis systems so that the structural information of enzymes in heterogeneous biocatalysis can be revealed and serve as a guide for the rational design of porous platforms for enzyme encapsulation.

RESULTS AND DISCUSSION

A brief introduction to EPR

Continuous-wave (CW) EPR, the most commonly seen EPR, detects the absorption of microwave radiation by samples containing paramagnetic species. Different from optical spectroscopy, in EPR, the paramagnetic sample is hosted in a resonator, which "reinforces" the microwave energy to enhance the absorption of the radiation. Usually, resonators are cavities formed by a metal box, although other types of resonators are available.[63,64] Without a paramagnetic sample, all microwave radiation will be reflected back by the resonator. Upon loading of a sample, its position can be

[1]Department of Chemistry and Biochemistry, North Dakota State University, Fargo, ND 58102, USA

[2]Department of Plant Sciences, North Dakota State University, Fargo, ND 58102, USA

[3]Research Computing, Information Technology at Purdue (ITaP), Purdue University, West Lafayette, IN 47907, USA

[4]Department of Chemistry, Purdue University, West Lafayette, IN 47907, USA

[5]Lead contact

*Correspondence: zhongyu.yang@ndsu.edu

https://doi.org/10.1016/j.checat.2021.03.005

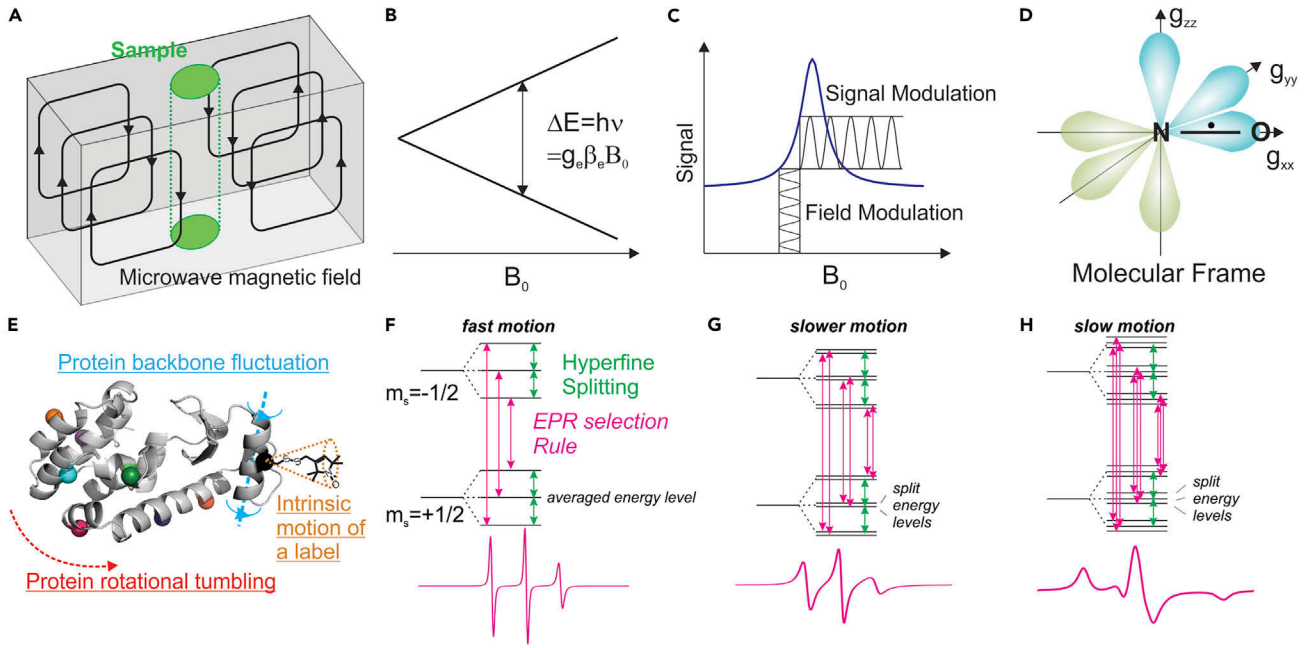

Figure 1. Basis of EPR principles and application in protein dynamics

(A) A typical design of an EPR cavity resonator. The sample is placed in the green cylinder.

(B) EPR transition frequency, ν, is proportional to the external magnetic field, B_0.

(C) Illustration of field modulation, which results in first-derivative peaks.

(D) Definition of the molecular frame of a nitroxide spin center, which approximately overlaps the p orbitals of the nitrogen atom.

(E) Three typical motions that can affect the EPR signal.

(F–H) Conceptual illustration of the effects of protein motion on the energy level splitting and resultant EPR transition linewidth. As the motion slows down, the linewidth becomes broader, resulting in an enhanced number of transitions allowed by the EPR selection rule.

tuned to the maximum magnetic field (minimum electric field) in the resonator (Figure 1A) so that the radiation is "concentrated" on the sample, leading to an absorption (often shown as a tuning "dip"). Note that the microwave radiation can penetrate the backgrounds of and be absorbed by all paramagnetic spin centers within the effective region of the resonator. Thus, EPR can detect the unpaired electrons in the entire ensemble of the sample regardless of sample phase and heterogeneity. It is cautioned that for aqueous protein samples, the sample and water volume should be properly selected. This is because the water molecules have a high imaginary part of the complex permittivity at microwave frequencies, leading to additional absorption and reduced cavity quality factor. The real part of water permittivity is also high, leading to field redistribution within the cavity.[34,35] Thus, practically, the sample diameter and volume should be sufficiently small. Reduced sample volume usually does not affect the signal strength given the high sensitivity of most modern EPR spectrometers.

For a free electron, an EPR transition occurs according to the following equation:

$$h\upsilon = g_e \beta_e B_0,$$

where υ is the frequency, B_0 is the external magnetic field, g_e is the g factor of the electron spin (2.0023), h is the Planck constant, and β_e is the Bohr magneton (Figure 1B). The most commonly seen EPR spectrometer is at the X band, which has ~0.34 T field and thus ~9.6 GHz absorption. Therefore, X-band EPR in principle is sensitive to motions on the order of subnanoseconds to tens of nanoseconds (reciprocal of the frequency). In most EPR spectrometers, a field modulation is needed because the

magnetic field is generated by alternating current (AC), and it is difficult to control the absolute AC and corresponding field. Instead, the change in the amplitude of the current over a short duration can be determined accurately. Thus, in most EPR spectrometers, the amplitude of absorption change is plotted over the modulated field, scanning over the latter of which results in the first-derivative spectrum (Figure 1C).

Practically, the electron has to be hosted or delocalized in an orbital, the nature of which also decides the resultant EPR signal. In general, nitroxide spin labels with an average g factor of ~2.0067 are the most commonly used for detecting protein dynamics at room temperature, although other paramagnetic species are also possible.[44,65–67] For a nitroxide spin center, the spin-orbital coupling makes the g factor orientation dependent. The resultant g tensor can be expressed as a 3 × 3 matrix:

$$\begin{pmatrix} g_{xx} & g_{xy} & g_{xz} \\ g_{yx} & g_{yy} & g_{yz} \\ g_{zx} & g_{zy} & g_{zz} \end{pmatrix},$$

which is a square matrix with the diagonal elements of g_{xx}, g_{yy}, and g_{zz} in the molecular frame (overlaps with the nitrogen p orbitals; Figure 1D).[68] In addition, the magnetic dipole-dipole coupling between the electron and the nuclear spins, the hyperfine interaction, contains an orientation-independent term, the Fermi contact, as well as an orientation-dependent term. This results in the hyperfine or A tensor, whose coordination approximately overlaps the nitrogen p orbitals as well:

$$\begin{pmatrix} A_{xx} & A_{xy} & A_{xz} \\ A_{yx} & A_{yy} & A_{yz} \\ A_{zx} & A_{zy} & A_{zz} \end{pmatrix}.$$

The final EPR absorption depends on the relative orientation of the molecular frame and the external magnetic field as well as the motions that can affect these orientations.

At room temperature, where proteins retain conformational flexibility and dynamics for function, three motions—rotational tumbling of the protein (correlation time τ_r), backbone fluctuation at the labeled site (correlation time τ_{bb}), and intrinsic motion of the spin label (correlation time τ_i)[69]—can change the relative orientation of the molecular frame with respect to the field (Figure 1E).[30,68] In this resource article, because we are focused on enzymes immobilized in mesoporous materials, the rotational tumbling time (τ_r) of the enzyme is sufficiently long such that the only contributions to the spin label's motion are the domain motion at the labeled site and the intrinsic motion of the R1 side chain.

For an enzyme placed in a buffer without any immobilization, in order to use CW EPR to determine protein structural information, the contribution from enzyme rotational tumbling should also be sufficiently long (τ_r > 20 n).[69] τ_r depends on the enzyme size and the buffer viscosity. For a protein with a molecular weight of ~20 kDa at room temperature in water, τ_r is ~6 ns. In this case, the τ_r can be increased to 20 ns by being mixed with common viscogens such as sucrose or Ficoll (30% or 25% w/w, respectively). A caution is that the osmotic and crowding effects can influence enzyme conformation and should be carefully analyzed.[70]

In addition to the rate of motion, the order of the motion of the spin label, S, which describes the angular amplitude of an anisotropic motion (S = 0, isotropic motion; S = 1, extremely anisotropic motion), can also influence the EPR spectrum. The detected ensemble EPR spectrum depends on the rate and order (spatial restriction) of the net effect of these motions. For a free protein in solution, the rapid rotational tumbling averages out the orientation-dependent terms of the A tensor. The

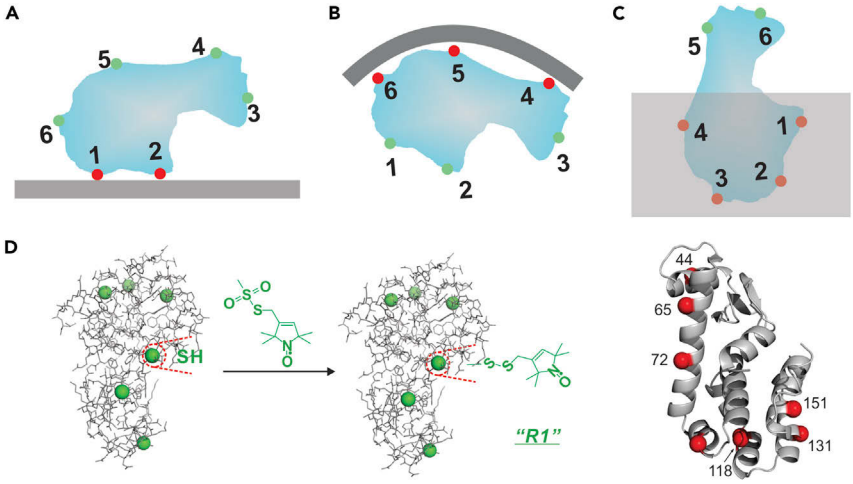

Figure 2. Site selection and SDSL reaction

Multiple enzyme surface sites are needed in order to pinpoint the relative orientation of the enzyme on the surface of a flat (A) or curved solid (B) or if the enzyme is partially entrapped in porous materials (C).

(D) Reaction of SDSL of an enzyme with the most popular labeling reagent to generate the R1 side chain. Surface residues are often selected, one at a time, to provide multiple contact points for orientation detection.

hyperfine splitting of each spin state (m_s = +1/2 or −1/2) becomes three energy levels separated by only the Fermi contact. The EPR selection rule thus leads to three transitions and an EPR spectrum with three shape peaks (Figure 1F). Upon immobilization on a solid support, protein rotational tumbling is "frozen," resulting in broader energy levels separated by the sum of the Fermi contact and the orientation-dependent terms of the hyperfine tensor, leading to a broader spectrum (Figure 1G). Upon contact with a solid surface with the labeled site (e.g., MOF and COF backbone), all three motions are restricted, resulting in an even broader spectrum (Figure 1H). On the basis of these principles, enzyme behavior can be probed at the molecular level or even higher resolution. In heterogeneous systems, the contribution from each motion can be reflected in the resultant spectrum.

Extending SDSL-EPR to heterogeneous biocatalysis

Extending SDSL-EPR to heterogeneous biocatalysis requires some special planning. Here, we summarize a brief procedure to cover most of the needed considerations based on our experience (Scheme 1). Depending on the enzyme, mesoporous materials, and/or purpose of study, certain steps can be skipped or further expanded.

Step 1: SDSL of the target enzyme

Step 1.1: Selection of the labeled site. The general strategy to determine the orientation of an enzyme in a nanoscale mesopore is to identify the regions and residues that contact the pore walls or scaffolds (Figures 2A–2C) so that the enzyme "sits" on the solids via these residues while pointing the rest away from the contact surface. Thus, multiple enzyme surface residues should be selected for labeling depending on enzyme size and number of subdomains. Typically, we select one residue for each helix or β strand. For example, for one of our model proteins, T4 phage lysozyme (T4L), we usually selected six to eight sites that cover most of the protein surface regions (Figure 2D).[20,61] Depending on the length of the helix or strand, more than one residue might be needed.

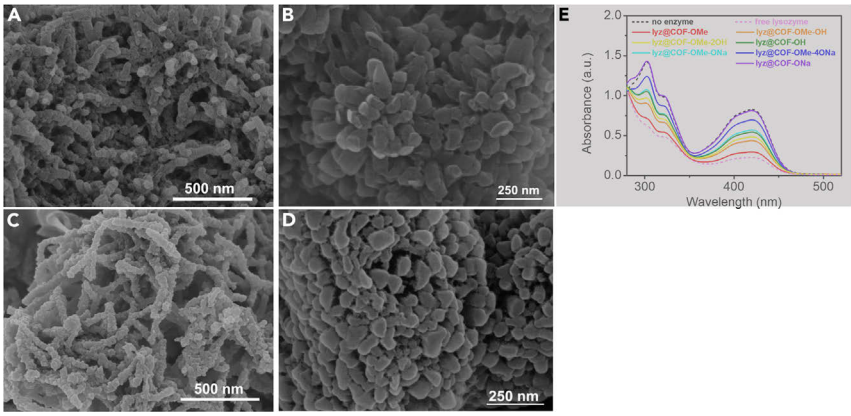

Figure 3. Enzyme location and activity characterization prior to dynamics and orientation measurements

One way to confirm the location of the enzyme in a compartment is the morphology. Scanning electron microscopy (SEM) images of COF-OMe in the absence (A) and presence (C) of lysozyme enzyme show identical morphology, suggesting that the enzyme is loaded into the pores of COF-OMe. Similarly, SEM images of COF-OH in the absence (B) and presence (D) of lysozyme also show identical morphology.

(E) The activity assay is needed to confirm that the entrapped enzyme is active, keeping in mind that small substrates are required to diffuse into the nanoscale pores.

Step 1.2: Site-directed mutagenesis. Site-directed mutagenesis allows amino acids to be replaced, inserted, or deleted in proteins within 1–2 weeks. In SDSL, we replace the native residue(s) of interest with a cysteine instead of inserting new residues to minimize alteration to the host enzyme. One caution is that the free native cysteines of the enzyme, unless participating in disulfide bonds, should be mutated to a serine or alanine to avoid labeling at undesired positions. This does not generate a large amount of additional work given the low natural abundance of cysteine.[69] For a cysteine-rich enzyme, an unnatural amino acid can be employed (see below). Another caution is that each site of interest needs to be mutated one at a time because the CW EPR spectra of the nitroxide spin label overlap one another if more than one label is attached, making it difficult to distinguish the contribution from each. This, meanwhile, is also not a hurdle given that multiple mutants can be prepared simultaneously, whereas the rate of CW EPR data acquisition is rapid (5–30 min per sample).

Step 1.3: EPR spin labeling. The cysteine mutants of the target enzyme prepared above are expressed and purified one at a time. The caution is that during purification, a reducing reagent (e.g., 5 mM dithiothreitol or tris(2-carboxyethyl)phosphine) is needed in the buffers to prevent protein dimerization and is removed via desalting right before reacting with a labeling reagent.[71] The best nitroxide labeling reagent is (1-oxyl-2,2,5,5-tetramethylpyrroline-3-methyl)methanethiosulfonate (MTSSL) because of its small size (such as a lysine), which minimizes the perturbation to the protein.[30,69] For a surface cysteine, the reaction usually completes within 20 ms under a 10-fold excess of MTSSL. Although partial labeling does not affect the EPR spectra, because unlabeled proteins are EPR silent, we usually strive to ensure complete labeling (e.g., reacting overnight at 4°C under foil cover). Excess MTSSL needs to be removed completely via filtration-centrifugation or desalting.

Step 1.4: Ensure the integrity of the labeled enzyme. To do so, we usually determine the molecular weight and purity, secondary structure, and activity via

electrophoresis, circular dichroism, and the standard activity assay, respectively. Should a mutation or label generate a major disturbance to the protein, a nearby residue (e.g., in the adjacent helical turn) should be selected for labeling in order to represent the same region or subdomain. Once labeled, each enzyme mutant is usually stocked at 0.2–0.5 mM to avoid protein aggregation (this can differ depending on the enzyme).

Step 2: Loading enzymes

Depending on the porous materials, the labeled enzymes can be loaded via either diffusion or co-precipitation (as in the case of enzyme@ZIF).[11] The reaction condition is mild (to retain enzyme stability) in a proper aqueous buffer that does not react or disturb the porous materials. In our best experience, HEPES buffer works well for most MOFs and COFs. Gentle shaking is suggested to enhance the loading efficiency. The loading should be monitored according to the enzyme concentration in the supernatant over time to ensure the completion of loading. Most MOFs and COFs can be saturated in 30 min to 2 days. All unloaded enzyme should be removed via centrifugation and resuspension.

This step is also the time to confirm the location or position of the enzyme. For porous materials, if the desired location is in the mesopores, then the morphology and surface charge of the materials should be retained before and after loading. For example, in a recent study, we found identical net surface charge and morphology of three COFs before and after enzyme loading, indicating that the enzyme was encapsulated into the channels of COFs (Figures 3A–3D).[62] Characterizations of MOFs and COFs are also necessary to confirm that enzyme loading does not disturb the materials. Should there be additional enzymes adhered to the surface of the materials, gentle sonication and extensive wash are often sufficient to remove them.

Step 3: Confirm enzymatic activity

The caution is to ensure that the substrate can sufficiently contact the enzyme. For example, lysozyme's physiological substrate is bacterial cell walls, which cannot diffuse into the pores of most mesoporous materials. Thus, in our study of lysozyme in COFs, we chose a small substrate, 11-chitosan, to evaluate the activity (Figure 3E).[62] On the other hand, when attempting to entrap enzymes on the surface of MOFs (for partial enzyme exposure and partial protection; see below), we directly use the commercial bacterial cell walls because the enzyme can contact the cells directly.[20]

Step 4: Acquire CW EPR spectra

Step 4.1: Instrumentation. Most of our orientation and dynamics studies were conducted on a CW EPR spectrometer (Varian E-109), which is also accessible at several national and regional EPR centers and Bruker Biospin. Typical brands and models include the Varian series (E-4 and E-109), Bruker E-580, Bruker EMX, and some benchtop spectrometers. For each measurement, ~1 μg of protein is needed in the porous materials after the removal of surface-adsorbed proteins. The sample holder has to be diamagnetic; we found borosilicate tubes to be the most accessible at a reasonable cost. At room temperature, the rapid tumbling of water magnetic dipoles can influence the absorption of microwave radiation by the sample. Thus, the amount of water should be minimal. We found tubes with 0.6 i.d. × 0.8 o.d. (available at Wilmad-LabGlass) and 2 cm height to be a good combination to minimize water influence while offering sufficient signal. Depending on the equipment, the sample volume can vary.

Step 4.2: Key spectral acquisition considerations. The first step of data acquisition is to tune the sample position to ensure the maximal absorption of the radiation

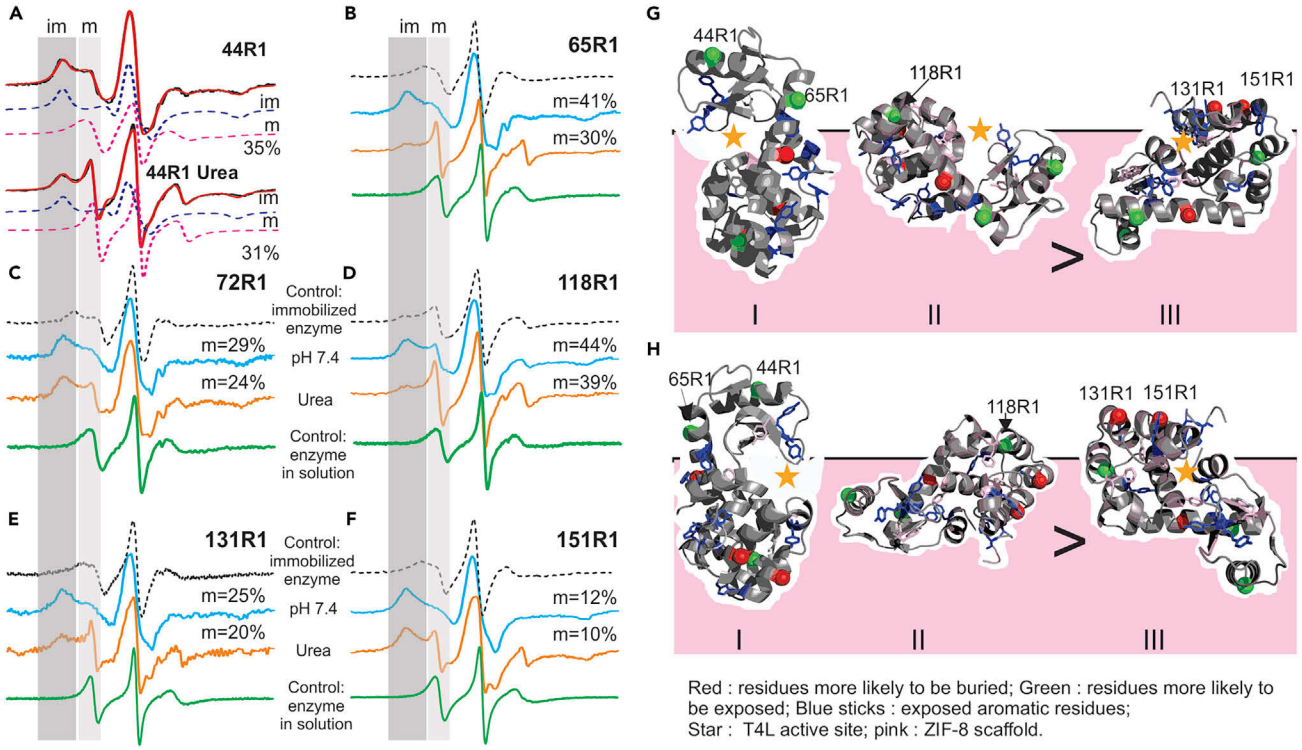

Figure 4. EPR data of lysozyme upon encapsulation in ZIF-8 and relative orientation on ZIF-8 surface

(A) CW EPR data (black) of 44R1 in the absence (top) and presence (bottom) of urea perturbation and associated spectral simulations (red). The two components indicated by im and m were deconvoluted as shown by the dotted curves.

(B–F) Five additional lysozyme sites were studied with CW EPR upon SDSL in solution (green), in ZIF-8 (cyan), and in ZIF-8 and urea (orange) and upon immobilization on a solid, non-porous surface (dotted). The percentage of the m component is labeled for each multi-component trace.

(G and H) The proposed enzyme orientation on the ZIF-8 surface based on the relative population of labeled sites. Adapted from Pan et al. with permission.[20]

(Figure 1A). This can usually be leveraged by the tuning catalog wherein a symmetric and deep "tuning dip" is reached upon adjusting the sample position. A nitroxide spin label results in 50–75 G wide spectra depending on the protein state, which leads to a typical scan range of 100 G. A 1 G field modulation is sufficient for nitroxides, although 0.2–0.5 G can also be used to probe the sharp peaks when protein partial unfolding with urea is employed (see below). Signal averaging is often needed to enhance the signal-to-noise ratio (SNR). Most modern EPR spectrometers have the autosummation function so that the spectrum of each scan is the average of all scans before. Each scan usually takes 30–60 s, and 5–30 min is often needed to acquire a spectrum with sufficient SNR (e.g., 20–30) for spectral simulation or analysis.

Step 4.3: CW EPR line shapes. A typical CW EPR line shape of a spin-labeled protein is a three-peak, first-derivative spectrum (see above). Because a labeled protein site in a sample can contact the pores and scaffolds in some molecules and not in others, we often observe clearly separated spectral components (as a result of their significantly different rates and orders of motion; Figure 4). We define the contact peak as "im," standing for immobilized, and the non-contact peak as "m," standing for mobile. Therefore, in a real sample, for the whole ensemble, a complex, two-component EPR spectrum is resolved; the contribution from each component can be deconvoluted via spectral simulation (Figure 4A).

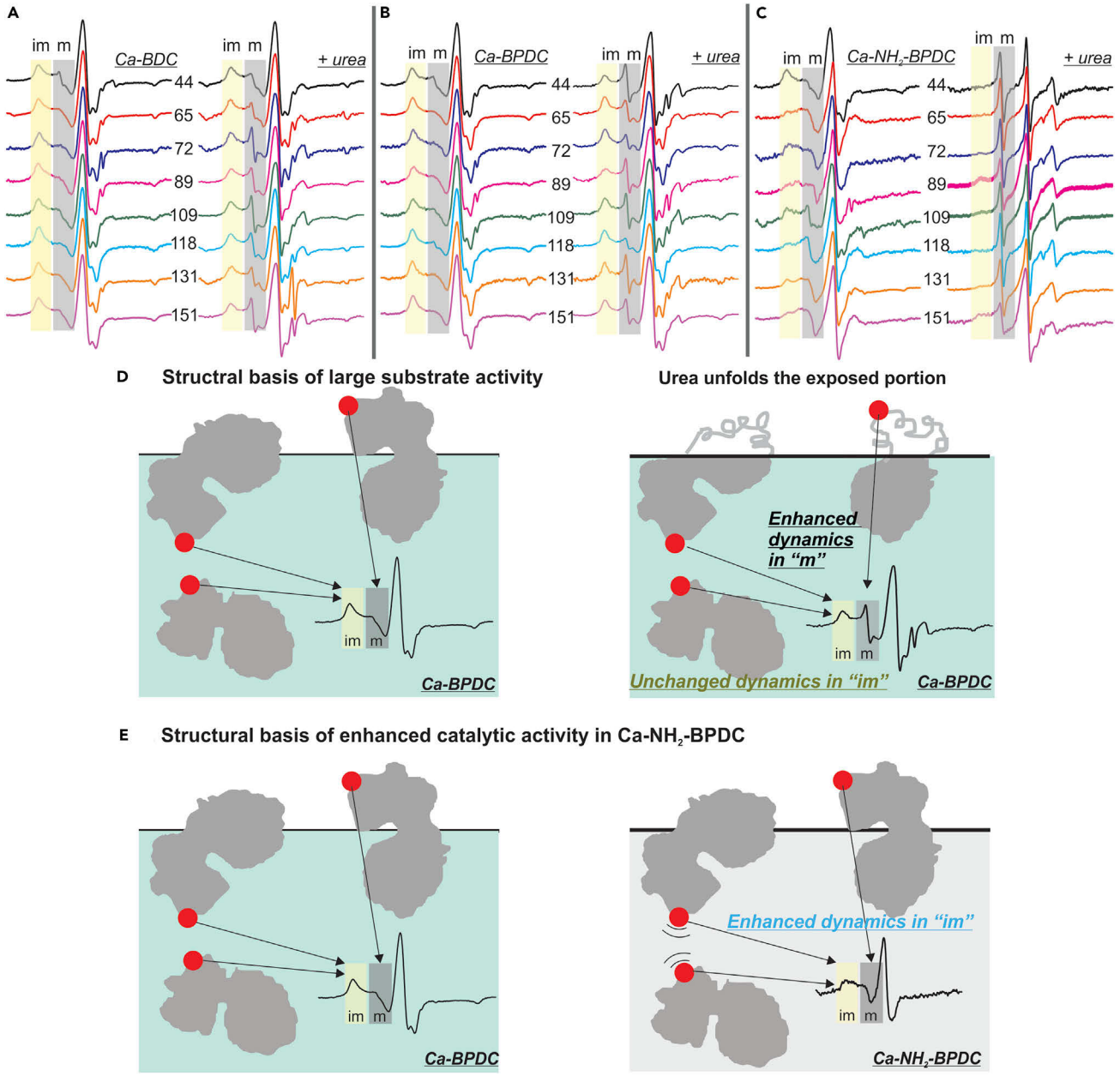

Figure 5. Probing the structural basis of the catalytic performance of enzyme@Ca-MOM composites

(A–C) EPR spectra of all labeled sites in the absence (left) and presence (right) of urea for lys@Ca-BDC (A), lys@Ca-BPDC (B), and lys@Ca-NH_2-BPDC (C). Shading indicates the two spectral components discussed in the text. Spectral range: 3,300–3,400 G.

(D) Illustration of EPR detection of the exposed (m component) and buried (im component) enzyme upon encapsulation on MOM surfaces (left) and upon treatment with urea, which unfolds only the exposed portion of the enzyme (right).

(E) Illustration of EPR detection of the backbone dynamics of the buried (im component) enzyme. Adapted from Pan et al. with permission.[61]

For example, in our recent work, we found two components for all sites of T4L studied in a zeolitic-imidazolate framework (ZIF-8; Figures 4A–4F),[20] a series of Ca-based metal-organic materials (MOMs; Figures 5A and 5B),[61] and COFs (Figure 6A).[62] The complex spectra were caused by the contact of the labeled site with the scaffolds of ZIF-8 and Ca-MOMs and the inner walls of COF channels, resulting in the im peaks, whereas the non-contact component yielded the m peaks.

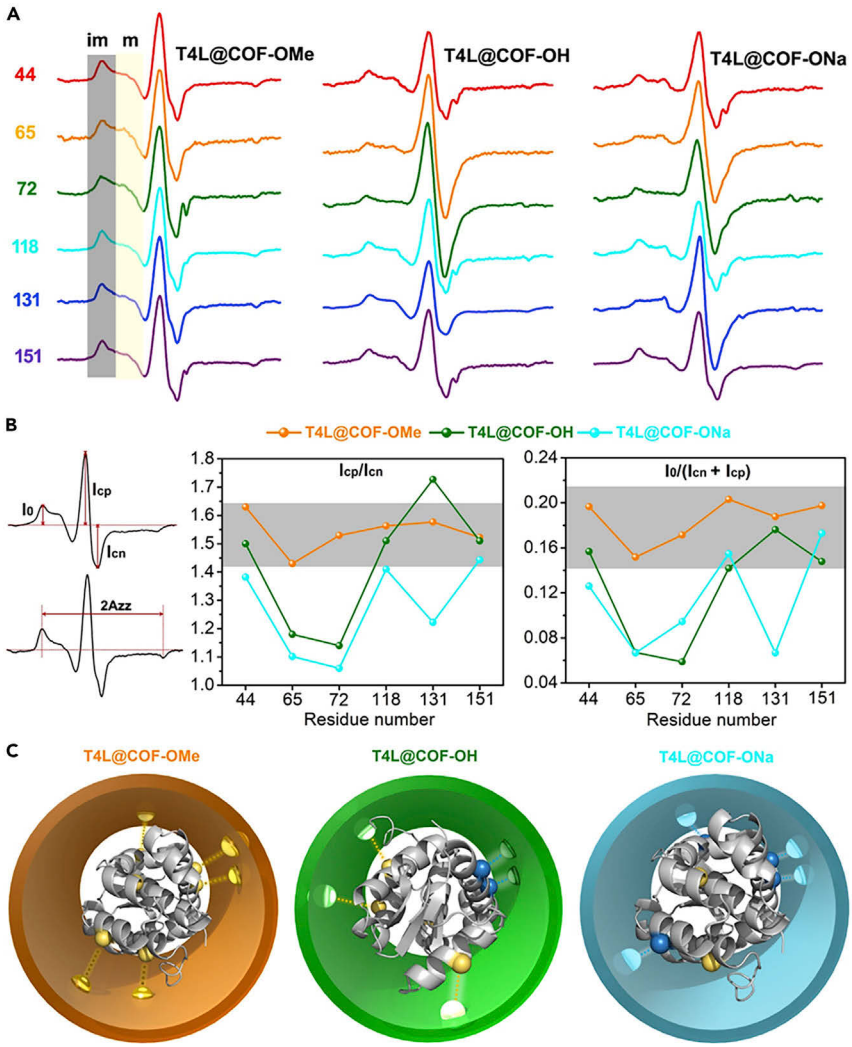

Figure 6. COF EPR data and deconvolution and orientation

(A) The EPR spectra of six labeled sites upon association with COF-OMe, COF-OH, and COF-ONa. Gray and yellow shading labeled im and m represent the immobile and mobile spectral components, respectively.

(B) Definitions of the three variables relevant to spin-exchange narrowing and illustration of measurement of the key parameter (A_{zz}) associated with the hydrophilicity of the immobile component of each labeled site. A quantitative description of the extent of spin-exchange narrowing using the ratio of the positive and negative peaks of the centerline (I_{cp}/I_{cn}) and the ratio of the amplitude of the low-field peak and that of the centerline peak ($I_0/(I_{cp} + I_{cn})$) is provided. Gray areas indicate typical parameter regions where no spin-exchange narrowing occurs, and lines are guidelines for the eyes.

(C) The proposed host-guest interactions of the enzyme after association with various COF materials derived from the EPR results. Yellow spheres indicate labeled sites with weak interactions with the COF channels, and blue spheres represent sites that strongly interact with the channels. Stronger host-guest interactions were detected in COF-ONa, followed by COF-OH and COF-OMe. Adapted from Sun et al. with permission.[62]

Step 4.4: EPR data interpretation. Spectral simulation is very important for interpreting the obtained EPR data and determining the parameters related to protein motion and dynamics. In principle, determining the parameters of the spin label's motion would require CW EPR at multiple frequencies and/or under varied viscosity conditions.[72–75] However, for the R1 spin label attached to the solvent-exposable α

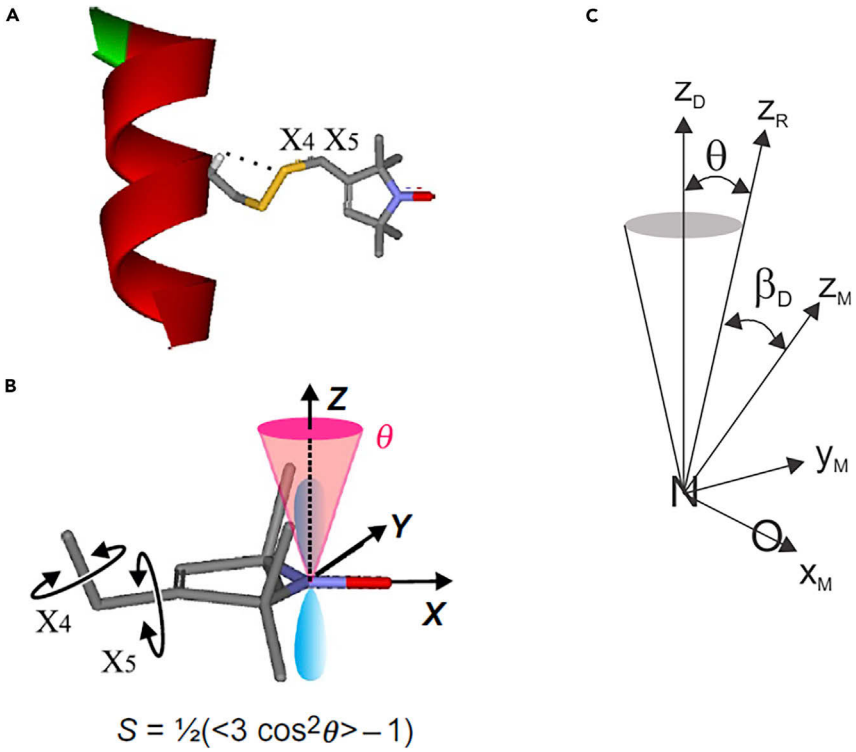

Figure 7. Known modeling basis of R1 label on a helix surface

(A) The structure of the R1 label on a helix. Two dihedral angles, χ_4 and χ_5, contribute to the averaging.

(B) Rotations around χ_4 and χ_5 lead to anisotropic averaging in a cone. The order parameter is dependent on angle θ.

(C) Definition of the three coordinate systems (Z_D, Z_R, and Z_M) related to the MOMD model. Adapted from Altenbach et al. with permission.[69]

helices of a small protein, e.g., T4L, the motion has already been understood to a certain level, including the crystal structure of the R1 side chain (Figure 7A), the typical ranges of the rate (τ) and order (S) parameters of R1 on α helices, and how these parameters change upon protein rotational tumbling changes.[70,76,77] Herein, the R1's crystal structure helps us understand the origins of the "anisotropic" motion of the spin label (Figure 7B).[69] On the basis of this knowledge, we carried out our simulation by using the established parameters (see below), which are highly likely to be reliable and accurate. However, for an unknown protein labeled at a non-helical region, X-band CW EPR together with multi-frequency EPR and varied viscosity conditions are suggested to accurately determine the rate and order parameters of the spin label, minimizing the potential errors.[72] High-field and high-frequency EPR spectrometers are currently available at multiple facility centers or labs.[37,78]

The most widely used EPR simulation algorithm is that developed by Freed and co-workers on the basis of the macroscopic-order microscopic-disorder (MOMD) model, which relies on the spatial ordering potentials for the motion of R1.[68] Herein, we varied the rate and order parameters of the spin label's motion within a cone space (as well as the relative populations in the case of more than one R1 dynamic mode) systematically to simulate the spectrum until the best fit was reached (Figure 7C). The detailed description of the algorithm is provided in the supplemental information. A few open resources, such as EasySpin and Multicomponent, are available for carrying out the simulations.[69,79] We chose Multicomponent, created by Dr.

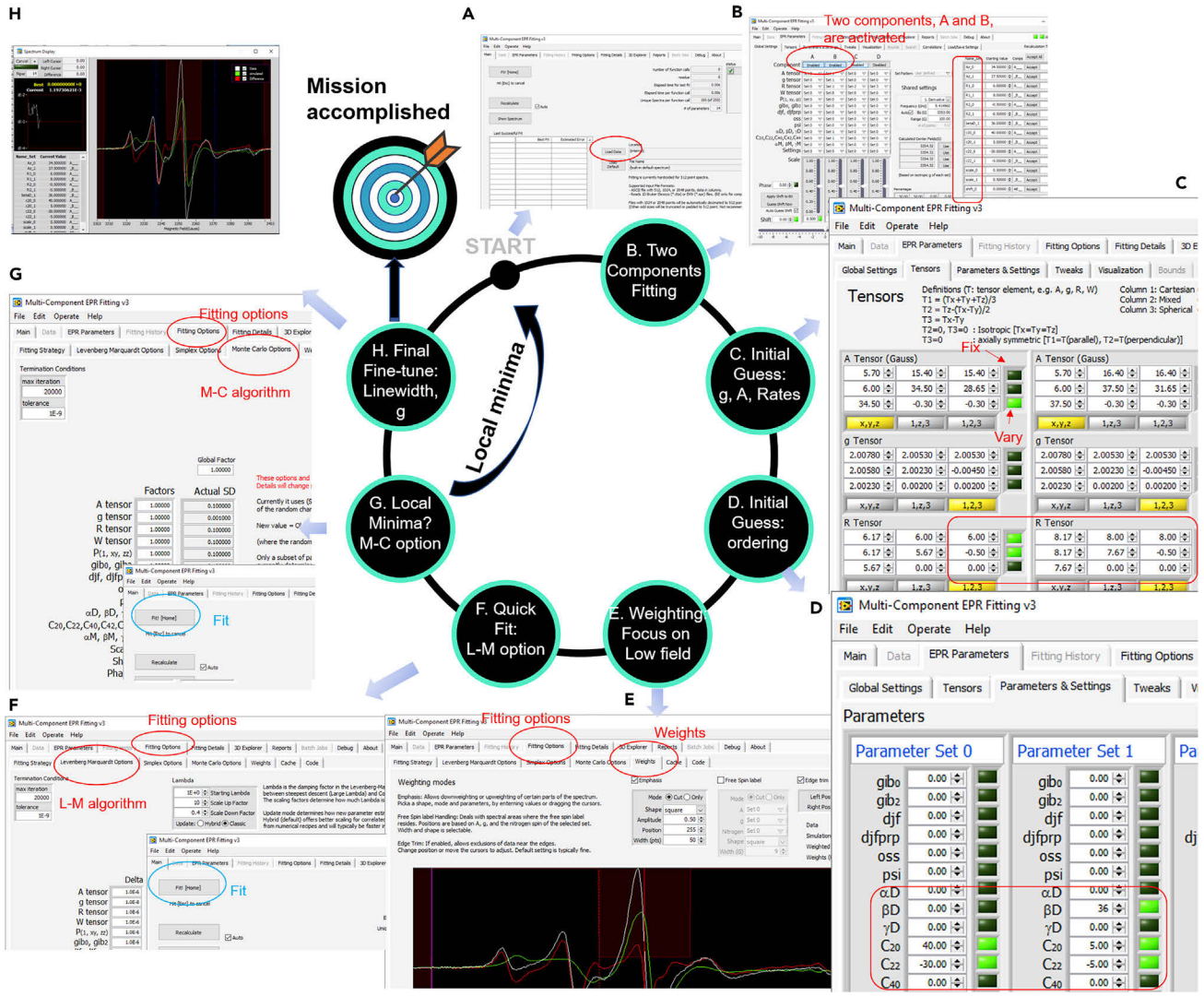

Figure 8. A general fitting procedure and the user interface at each key step of the simulation program

The "light" after each parameter indicates whether the parameter can be varied or fixed during the simulation. For details, see the main text.

Altenbach and available at his website: https://sites.google.com/site/altenbach/labview-programs/epr-programs/multicomponent (user interface; see Figure 8). A general procedure typically adapted in our data analysis is shown in Figure 8. In particular, a careful baseline correction and signal normalization are needed prior to simulation. Then, the data are loaded into the Multicomponent software (Figure 8A), where two components are activated to simulate the im and m components (components A and B for im and m, respectively; Figure 8B). Switching tab to "tensors," the initial guesses of the g and hyperfine tensors, as well as the rate parameters, are g_{xx} = 2.0078, g_{yy} = 2.0058, and g_{zz} = 2.0023 for both im and m components; A_{xx} = 5.7 G and A_{yy} = 6.0 G for both im and m components; and A_{zz} = 34.5 and 37.5 G for the im and m components, respectively. In the rate tensor (due to anisotropy), the R values instead of the actual effective correlation time, τ_i, of R1 diffusion are the input, wherein $1/6R = \tau_i$. The R tensor is defined in Figure 8C, where the average constant, R_1, is $(R_x + R_y + R_z)/3$, R_2 is $R_z - (R_x - R_y)/2$, and R_3 is $R_x - R_y$. In fact, in the program, all tensors (g, A, and even the line-width tensor, W) can be defined similarly.

For our case, where an axial symmetry is assumed, R_1 and R_2 are non-zero. The average rate constants, R_1, of 6.00 and 8.00 are often input for the im and m components, respectively, with −0.5 to account for the anisotropic motion of both components, R_2 (see Figure 8C). The g values and A_{xx} and A_{yy} are often fixed, whereas A_{zz} and the rate tensors are allowed to vary during the simulation (as indicated by the activated green light). Next, key ordering parameters need to be put in (Figure 8D). A restoring (ordering) potential (U) is appropriate to describe the extent of spatial constraints of the spin label within the "cone."[68] The restoring potential $U(\theta) = -1/2k_BTc_0^2\,(3\cos^2\theta - 1)$ + HOT, where c_0^2 is a scaling coefficient and HOT represents higher-order terms.[68] The spatial ordering of the diffusion tensor, S, can be computed according to Figure 7B. In our simulations, only the dominant term and the first HOT were involved, leading to the order parameters S_{20} and S_{22} , which can be computed from the C_{20} and C_{22} coefficients, respectively (Figure 8D). For the im component, because of the strong contact of the label with some species (e.g., the surface of mesopores), typical initial C_{20} and C_{22} are approximately 40 and −40, respectively. For the m component, we find that 5 and −5 are usually good initial guesses for C_{20} and C_{22}, respectively. The tilt of the diffusion tensor with respect to the molecular axis of the nitroxide is specified by the Euler angles (α_D, β_D, and γ_D). For axially symmetric motion, only β_D and γ_D need be specified. For z axis anisotropic motion, the diffusion tilt was fixed at $\beta_D = 36°$, $\gamma_D = 0°$. C_{20} and C_{22} for the two components and β_D are allowed to be altered during the simulation (see the green light after each variable). Practically, the A and g tensors do not always overlap, resulting in non-collinear tensors, which can be taken into account by another three Euler angles. Such an action will certainly make the simulations more accurate but extend the simulation time. Furthermore, such an effort usually does not yield noticeable differences in the final rate and order parameters in the simulation. Thus, we usually assume collinear A and g tensors in the simulation. Usually the low-field region of the spectrum is the most informative area; thus, the central peak is weighted by 50% (Figure 8E). Upon setting up all these parameters, we carry out a Levenberg-Marquardt fit to quickly determine the parameters that best fit the spectrum (finding a minimal χ^2; Figure 8F). Often, this is followed by the Monte Carlo fitting option in order to avoid falling into the local minima (Figure 8G). Finally, other parameters such as the line-width tensor W (Figure 8G) are allowed to change to fine-tune the fitting.

Step 5: Determine enzyme-relative orientation

Case I: Enzyme orientation in mesopores. On a solid surface, with either a positive (e.g., nanoparticles) or a negative (e.g., porous materials; Figure 2B) curvature, we can determine the enzyme orientation by revealing the residues and regions that contact the surface.[80] Such a contact will generate a high restriction to the motion of the spin label, resulting in an im spectral component, the contribution of which can be distinguished from the m component via spectral simulation (see step 4.4), leading to the relative chance of each labeled site to contact. By scanning a number of protein surface sites, we will be able to identify which regions contact the solid surface, leading to the relative orientation of the protein.

Using this principle, we recently probed the encapsulation of T4L in a channel-shaped, hydrophobic compartment, COF-OMe.[62] As shown in Figure 6A, all six labeled surface sites showed an im and an m component (as highlighted by gray and yellow shades, respectively). Spectral simulations shown in our supplemental information indicate similar rate and ordering parameters for each site (i.e., $A_{zz,im}$ ~ 35.0 G, $A_{zz,m}$ ~ 35.5 G, $R_{1,im}$ ~ 5.85, $R_{1,m}$ ~7.70, $C_{20,im}$ ~ 48, $C_{22,im}$ ~ −50, and population of the m component ~ 50%). These data indicate that almost all labeled sites experience similar rate and

spatial restrictions in the motion of the spin label. Furthermore, the similar population in the im component suggests that almost all sites of T4L have a similar chance of contacting the inner walls of the COF-OMe channel, indicating a random orientation therein (Figures 6A and 6C). This is reasonable given the close sizes of the channel (3.4 nm) and the enzyme (2.5 × 3 × 5 nm), as well as the symmetric shape of the channel. This explains the observed catalytic activity, wherein the active site of at least some enzyme molecules is accessible to the substrate, 11-chitosan, which can diffuse into COF-OMe and be hydrolyzed.[62] We are certain that the im components of the spectra shown in Figures 4, 5, and 6 originate from R1 in contact with the materials because of the negative controls carried out on each labeled mutant in buffer solution, which showed only an m spectral component. These results are consistent with the literature on T4L EPR investigations on various sites.[70,76,77,81]

Case II: Enzyme orientation on a MOF surface. An important approach to enzyme immobilization for large-substrate biocatalysis is to entrap enzymes in MOFs via co-precipitation, which results in partial exposure of some enzyme molecules on MOF surfaces and thus allows for contact with large substrates. A critical factor for this strategy to succeed is to ensure that the active site of the enzyme is sufficiently exposed and correctly oriented (toward the reaction medium). Thus, it is important to measure the enzyme orientation on a MOF surface. The principle is similar to that in case I of this step, where a protein residue buried under the MOF surface will possess significantly restricted backbone dynamics as a result of contact, whereas an exposed residue will display an m spectrum. The resultant spectra for an ensemble are also two-component spectra. We demonstrated this approach in a recent work wherein T4L was entrapped on a ZIF-8 surface. The EPR data shown in Figures 4A–4F for six surface sites labeled with R1 show both the im and the m components. Using a simulation procedure introduced in step 4.4, we were able to deconvolute the contribution of each component (see dotted curves in Figure 4A). Interestingly, the rate and order parameters of each labeled site were similar for both the im and the m components (i.e., $A_{zz,im}$ ~ 34.5 G, $A_{zz,m}$ ~ 37.0 G, $R_{1,im}$ ~ 6.00, $R_{1,m}$ ~7.90, $C_{20,im}$ ~ 45, and $C_{22,im}$ ~ −45; see the supplemental information of Pan et al.[20]). The major difference among different labeled sites was the relative population of the m component, wherein residues in the N terminus (such as 44R1 and 65R1) showed an ~25%–30% chance of being exposed. Also, residue 118R1 showed an ~40% chance of exposure. These are much higher than the N-terminal residues represented by 131R1 and 151R1, which tend to be exposed by ~10%–15%.[20] These findings suggest the preferential orientation of T4L on being entrapped on a ZIF-8 surface so that the N terminus and the 118R1 area have a higher chance of being exposed to the solvent than the N terminus. Such a high chance of exposing the N terminus was the origin of the catalytic activity because the active site is in close proximity (Figures 4G and 4H).

In our most recent work, we immobilized T4L in Ca-MOMs. Eight surface sites of T4L were labeled, and then EPR spectra were acquired. After spectral simulation, we found similar rate and order parameters for each labeled site for both the im and the m components when the enzyme was immobilized on Ca-BDC and Ca-BPDC (Figures 5A and 5B; $A_{zz,im}$ ~ 34.5 G, $A_{zz,m}$ ~ 37.0 G, $R_{1,im}$ ~ 6.10, $R_{1,m}$ ~ 6.60–7.10, $C_{20,im}$ ~ 40, and $C_{22,im}$ ~ −40; see Table S1 and the supplemental information of Pan et al.[61]). The major difference among different labeled sites was the relative population of the m component, wherein T4L had a higher chance (>50% of the m population) of exposing the N terminus in Ca-BPDC than in Ca-BDC (<40% of the m population), which explains the relatively high catalytic efficiency in the former (Figure 5A versus Figure 5B and Table 1).[61]

Table 1. Percentage of the m component of T4L entrapped in Ca-BDC and Ca-BPDC

	Percentage of m in Ca-BDC	Percentage of m in Ca-BPDC
44R1 (N terminus)	36.9%	52.1%
65R1	35.7%	29.2%
72R1	49.8%	35.4%
89R1	54.4%	41.2%
109R1	44.1%	36.9%
118R1	39.3%	33.5%
131R1	47.7%	49.6%
151R1 (C terminus)	50.0%	47.5%

In Ca-BDC, the N terminus (close to the active site) has a lower chance of being exposed than the C terminus, whereas both the N and C termini of the enzyme in Ca-BPDC have a high chance of being exposed.

This strategy in both works was further supported by a urea-perturbation test, wherein only the exposed residues were unfolded by urea, but the buried ones were unperturbed (Figure 5D). Such urea perturbation mainly resulted in an enhanced rate of the m component ($R_{1,m}$ increased from ~7.90 to ~8.40 in the ZIF-8 case but increased from ~7.00 to ~8.00 in the Ca-BDC/Ca-BPDC case). However, the relative population of the m population was close to that before urea addition for each mutant (within experimental error), whereas the motion of the m component was significantly enhanced, as judged by the sharp m peaks (Figures 4 and 5).[20] The caution here is that if the enzyme is encapsulated in relatively larger cavities or pores, urea could also unfold the portion of proteins inside of the MOF or COF. Therefore, the urea test is suggested primarily in the co-precipitation approach.

Step 6: Determine enzyme backbone dynamics of the contact residues

Case I: Probe the backbone dynamics difference. In addition to the fruitful orientation information underlying the m component, the im component is also worth probing. As introduced in steps 4.3 and 4.4, the rate and order of the im component are dependent on the local spatial restrictions and rate of rotational diffusion of the spin label. Both decide the backbone dynamics of the enzyme allowed at the labeled site and possibly the catalytic efficiency depending on how the labeled site is related to the active site and/or substrate recognition. Note that even if a labeled site is distant from the active site, the allosteric effect could still affect the overall catalytic performance.[40,82]

The most intriguing example is our recent work. In a specific Ca-MOM (named Ca-NH_2-BPDC in the article), three of four studied enzymes (lysozyme, lipase, glucose oxidase [GOx], and horseradish peroxidase [HRP]) displayed higher catalytic efficiency than Ca-BPDC, although the crystal scaffolds (determined via powder X-ray diffraction) and size of the composites were similar.[61] Because the substrates of lipase, GOx, and HRP are all smaller than the Ca-MOM pores, the catalytic performance must be primarily dependent on the enzymes buried within the MOM scaffolds. Thus, we investigated and compared the im component of a model enzyme, T4L, trapped in these two Ca-MOMs—Ca-BPDC and Ca-NH_2-BPDC—by using SDSL-EPR.[61] We found that although the rates of the m component in both Ca-MOMs for all studied sites were close ($R_{1,m}$ ~ 7.00–7.10), the rate and order of the im components for most labeled sites were different between the two Ca-MOMs. In particular, the rates of the im component of several labeled sites (i.e., 65R1, 89R1, 118R1, and 151R1) were enhanced to ~6.50 in Ca-NH_2-BPDC compared with ~6.00 in Ca-BPDC. Furthermore, the ordering parameters, C_{20} and C_{22}, were reduced to ~25.0 and −25.0 in Ca-NH_2-BPDC, respectively, compared with ~45.0 and −45.0, respectively, in Ca-BPDC. Thus, most labeled sites showed a higher

rate and lower order in the im peak in Ca-NH_2-BPDC than in Ca-BPDC. The enhanced enzyme dynamics could cause improved enzyme catalytic performance, which was proposed to be the cause of the high catalytic efficiency for the entrapped enzyme in the former Ca-MOM (Figures 5C and 5E).[61]

Case II: Spin-exchange interaction and "strength" of contact with the pores. The im component can also indicate the relative strength of the enzyme that contacts the compartment. For example, we found strong spin-exchange interactions in the spectra of some labeled T4L sites upon encapsulation in COF-OH and COF-ONa, which is indicated by the reduced peak intensity at the im region and the near-symmetrical central peak (Figure 6A).[62] This is in line with the expectation when spin exchange occurs so that the observed line shape looks like the "average" of the multiple spectra that are in fast exchange. The reason that spin exchange can occur in these two COFs is that, upon strong contact of a labeled site with the COF wall, the unpaired electron can enter the stacked π orbitals of the COF walls and be delocalized through the whole chamber. This electron can then be exchanged with another electron from another enzyme in the same chamber. Inspired by earlier works,[83,84] we utilized the relative peak intensity of the low-field peak versus the central line ($I_0/(I_{cp} + I_{cn})$), as well as the positive and negative peaks of the central peak (I_{cp}/I_{cn}; Figure 6B), to quantitatively assess the relative strength of the spin-exchange interaction. The smaller the $I_0/(I_{cp} + I_{cn})$, the stronger the exchange; the closer the I_{cp}/I_{cn} to 1, the more symmetrical the central peak and the stronger the spin exchange. Quantitively, we found that among all the EPR data we have on T4L encapsulation in three COFs (COF-OMe, COF-OH, and COF-ONa), an I_{cp}/I_{cn} larger than ~1.4 usually does not show serious spin exchange. Also, an $I_0/(I_{cp} + I_{cn})$ larger than ~0.14 does not generate serious spin exchange.[62] On the basis of these criteria, we determined the number of residues that show strong exchange interaction (and thus strong contact with the walls) to be 0, 2, and 4 in COF-OMe, COF-OH, and COF-ONa, respectively (Figure 6C). This trend is the opposite of the relative catalytic efficiency of lysozyme encapsulated in these three COFs, suggesting that the catalytic performance is related to the conformational degree of freedom of an enzyme upon encapsulation in porous materials so that the stronger the contact (or the more residues that strongly contact the pore), the higher the restriction in conformational flexibility and the lower the catalytic efficiency.

Other EPR labels

In addition to the R1 label, other spin probes and tags with different rigidity, attachment chemistry, and resonance properties have been developed for determining the structural and/or dynamic information in proteins.[60,85,86] For example, the RX label (see Figure 9), which reacts with two protein cysteines in close proximity (residues i and i + 4 on a helix or i and i + 2 on a β strand), significantly restricts the intrinsic flexibility of the label so that only the backbone motion affects the resultant spectra.[71] A direct application of RX was to determine the rate of the "rocking" motion of a helix of a protein by using an advanced EPR method: saturation recovery (SR; see below).[71] RX can also be applied in measuring distance distributions between two RX labels (and thus four cysteine mutations are needed) via double electron-electron resonance (DEER) EPR (see below). The results are often free of potential uncertainty caused by the label's intrinsic flexibility and can lead to more accurate backbone-backbone distances in a protein.[71] Finally, the restricted motion results in long relaxation times at room temperature (T_1 of RX on the order of 7–12 μs), which had been used for determining distances between RX and a fast-relaxing spin center via SR (see below; e.g., Cu^{2+}).[87] Similarly, R1p, R8, and V1 (see Figure 9) also possess relatively high restriction in the spin label's intrinsic motion and can be used for determining distances and backbone dynamics with reduced uncertainty caused by the label's

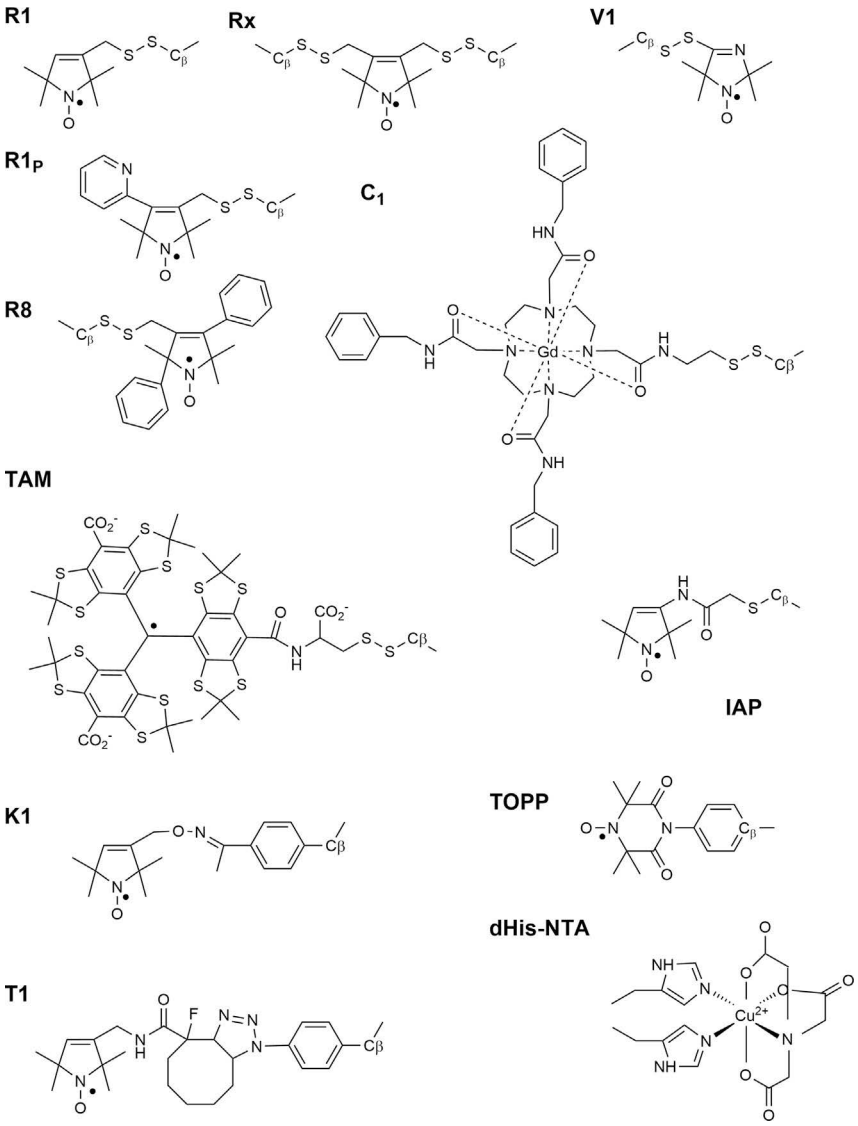

Figure 9. Commonly seen spin labels and probes for EPR studies
In each label, C_β connects to the C_α of a cysteine, unnatural amino acid, or histidine of a protein or peptide. The structure of R1 is presented for comparison.

intrinsic flexibility.[30,69] The TOPP label (see Figure 9) also contains highly restricted intrinsic motion.[86,88] In addition to nitroxides, other spin centers have been developed. For example, the trityl label (or the triarylmethyl [TAM] label), which can react with a protein cysteine (see Figure 9),[89] displays extremely narrow line width. Although TAM is not often used to probe the backbone dynamics of the labeled site, its long relaxation times at room temperature allow for determining distances in a doubly labeled protein at room temperature via SR or double quantum coherence (DQC).[57,87,89–93] Paramagnetic metals, such as Gd^{3+}, in a chelating compound can also be applied as a spin probe (see C1 in Figure 9)[39,65,94–97] for determining interspin distances in a protein. An advantage of the C1 label is the protective effect of the chelating compound, which allows for in-cell protein distance measurement.[39,65] Under reducing conditions, the 3-(2-iodoacetamido)-PROXYL (IAP) label, which does not form disulfide bonds and is therefore relatively stable under reducing conditions, can be used to attach to protein cysteines (see Figure 9).[86]

For a cysteine-rich protein, mutation of all native cysteines is often not ideal for protein function. Instead, unnatural amino acids become the choice of labeling. For example, *p*-acetylphenylalanine with a ketone-specific reagent (HO-4120) and *p*-azidophenylalanine have been demonstrated in protein spin labeling (see Figure 9) and EPR studies.[98,99] The labeling reagents often must be custom made. In addition, the Cu^{2+} labeling strategy based on double histidine and nitrilotriacetic acid compound can avoid the need for cysteine (see Figure 9).[100–102] Although Cu^{2+} has mainly been used in distance measurement, a recent contribution proved the use of Cu^{2+} for backbone dynamics measurements.[66] Mn^{2+} is another EPR spin probe demonstrated to be effective for distance measurement (see below).[103–105]

All these alternative spin labels and probes can potentially be used in the future research of heterogeneous biocatalysis to probe the backbone dynamics and global structural changes of enzymes (see below) entrapped in mesoporous materials. A caution is that compared with the popular R1, some alternative spin labels can possess different intrinsic flexibility and thus sensitivity to the backbone motion of the labeled site. However, upon contact with pore walls or MOF scaffolds, the motion of these alternative labels should also be highly restricted (and thus generate the im peak), which can still be useful for distinguishing the contact component from the non-contact component, leading to enzyme orientation information.

Intraprotein distance measurement using EPR

Although the backbone dynamics and relative orientation of the enzyme in porous materials are informative for revealing the underlying structural basis of the catalytic performance to a certain level, an important aspect of structural information—the large-scale structural changes—is also worth probing and will definitely improve the fundamental understanding of the functionality of the immobilized enzymes. EPR offers an excellent opportunity to probe for this information. The most powerful and widely used pulsed EPR technique, DEER, is an example. DEER measures the magnetic dipolar interaction between two spin centers (Figure 10A) separated by 2–8 nm.[36,38] Typically, a set of observe microwave pulses with the sequence ($\pi/2$-π-π) shown in Figure 10B are applied to excite a portion of the spins (Figure 10C) in the sample, and a "spin echo" is observed. Then a pump pulse is applied at a certain duration (t_p) after the second observe pulse, and a certain frequency, usually ~70 MHz, is offset to modulate the spin echo (Figure 10C). A typical DEER signal is an integration of the spin echo over t_p, which is an oscillating time domain signal (Figure 10D):

$$V(t_p) = \iint P(r)\xi(\theta)\langle 1 - \cos\left[\omega_{dd}\left(1 - 3\cos\theta^2\right) + J\right]t_p\rangle d\theta dr_{12}, \qquad \text{(Equation 1)}$$

where $P(r)$ is the distance distribution between the two spins, ω_{dd} is the magnetic dipolar interaction between the two spins, r_{12} is the distance between the two spins, θ is the angle between the vector of r_{12} and the external magnetic field, J is the exchange interaction between the two spins, and $\xi(\theta)$ is a factor depending on the relative orientation of the two spin centers. A Fourier transformation results in a Pake pattern, the frequency of which depends on the interspin distance, r_{12} (Figure 10E). When more than one distance is present in the target system, which is often the case of proteins as a result of the protein intrinsic conformational flexibility, each distance contributes to a set of peaks in the Pake pattern. Several user-friendly DEER data analysis packages are available to facilitate the rapid $P(r)$ extraction.[79,106,107] Therefore, analyzing DEER data, which extract both the distances and their relative probability between the two labeled sites, can reveal the conformational flexibility between the two labeled regions in a protein.[71,82,88,90,94,98]

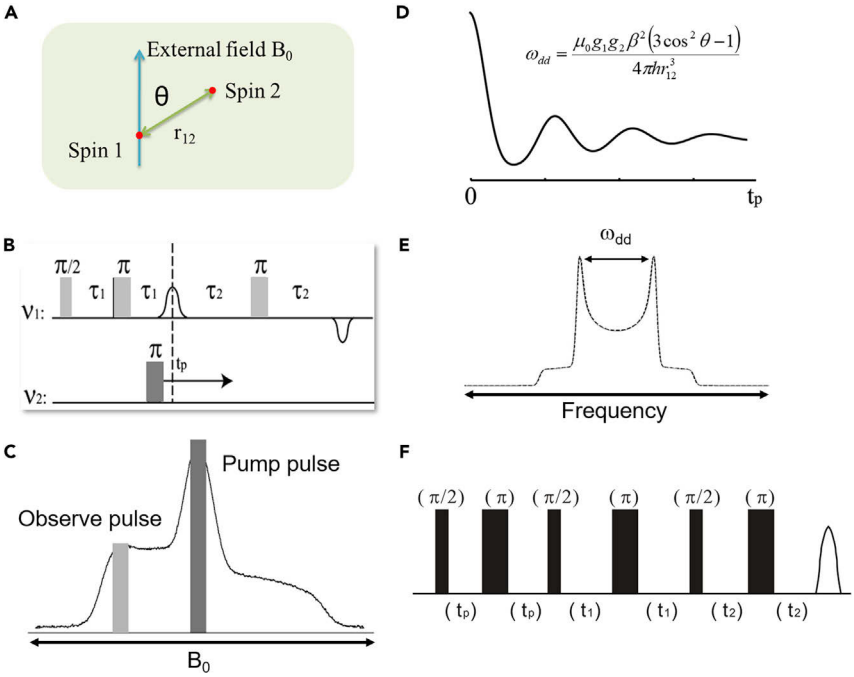

Figure 10. Pulsed methods to measure the distance distribution between EPR spin centers

(A) Illustration of two spin centers separated by a distance, r_{12}, in an external magnetic field, B_0. The angle between B_0 and r_{12} is θ.

(B) Pulse sequence of DEER.

(C) Illustration of the selective excitation of spins in a nitroxide-labeled system. The absorption spectrum is a typical field swept of nitroxides.

(D) A typical DEER signal caused by the magnetic dipolar interaction between the two spins. Variables: h is the Planck constant, r_{12} is the interspin distance, g_1 and g_2 are the g factors of the two spins, β is the Bohr magneton, and μ_0 is the vacuum permeability.

(E) A typical Pake pattern after the Fourier transformation of the DEER signal.

(F) The pulse sequence of DQC. The pulse lengths in DQC are usually much shorter than those in DEER.

A unique feature of DEER is an opportunity to extract the relative orientation of the spin centers due to the presence of the ξ(θ) term in Equation 1. This is especially important for rigid polypeptides, membrane proteins, and metalloproteins.[44,50,100,108–110] To probe the orientation effect, the general strategy is to acquire DEER signal at multiple magnetic fields with varied frequency offsets and then perform a global data analysis to simultaneously determine both $P(r)$ and ξ(θ).[107,111–113] The relative orientations of spin centers among nitroxide, TAM, and Cu^{2+} centers have been determined by this strategy.[50,111,114] Finally, the spin-exchange interaction (the J term in Equation 1) can also be separated from the dipolar interaction and determined, which yields more accurate distance information.[115–118]

In addition to DEER, DQC is another powerful pulsed dipolar spectroscopy to determine distance distributions between spin centers.[37,119,120] The advantage of DQC is the high sensitivity due to the use of six strong pulses (to excite a sufficient number of spins; Figure 10F), which also minimizes the orientation effects. The principles and applications of DQC can be found in several elegant reviews.[37,119]

As mentioned above, almost all spin labels discussed in Figure 9 have been demonstrated to be feasible for DEER and/or DQC applications. A caution is that a full data analysis procedure should be carried out when metal centers are studied by DEER so

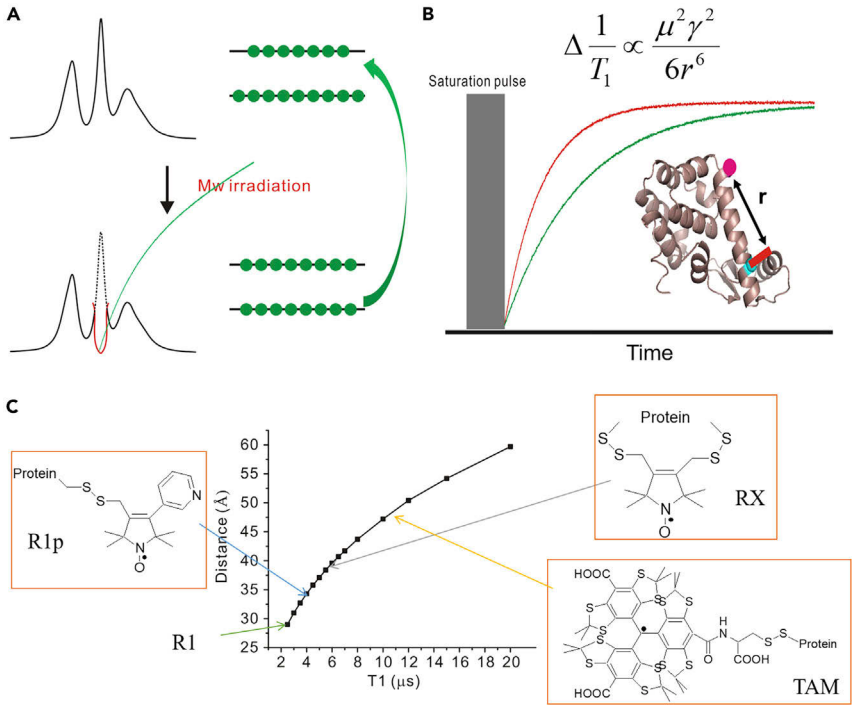

Figure 11. Saturation recovery-based interspin distance measurement

(A) Conceptual illustration of the principle of SR. A microwave pulse applied at the centerline of a nitroxide absorption spectrum "saturates" the population difference. Over time, upon removal of the pulse, the population difference is regained, and monitoring the signal re-gain results in an exponentially increasing curve.

(B) Illustration of the SR pulse sequence and typical SR signals for a slowly relaxing spin (e.g., a nitroxide) in the absence (green) and presence (purple) of a fast-relaxing spin.

(C) Typical spin-lattice relaxation time, T_1, at room temperature for three spin labels with restricted intrinsic dynamics.

that the orientation effect can be accurately taken into account. Note that although sample freezing and low temperatures are needed for pulsed dipolar spectroscopy (to delay the signal decay), it has been proved possible to measure $P(r)$ at room temperature by using spin labels with long relaxation times.[89,90]

Another pulsed EPR approach to determine distances in proteins is SR, which is based on the distance dependence of the enhancement of a spin label's relaxation rate (Figures 11A and 11B).[87,121–125] The principle is that the relaxation rate of a slowly relaxing spin label will be enhanced if a fast-relaxing spin is present in close proximity. The enhancement is proportional to $1/r^6$, where r is the distance between the two spin centers. Thus far, SR is able to determine only the average distances instead of the full distance distribution. The advantage of SR is that by using a few slow-relaxing nitroxide or TAM spin labels, it is possible to measure the average distances between spin centers at room temperature (Figures 11C),[122] which is useful for probing proteins under their physiological conditions. Typical applications of SR on distance measurements in proteins and peptides include metal ions such as Cu^{2+} and lanthanides employed as the fast-relaxing spin, whereas TAM or nitroxides have been used as the slowly relaxing center.[96,122,124–127]

For shorter interspin distances (e.g., <22 Å), CW EPR can determine the $P(r)$ at room temperature.[128] The principle is that two spins in close proximity would result in line

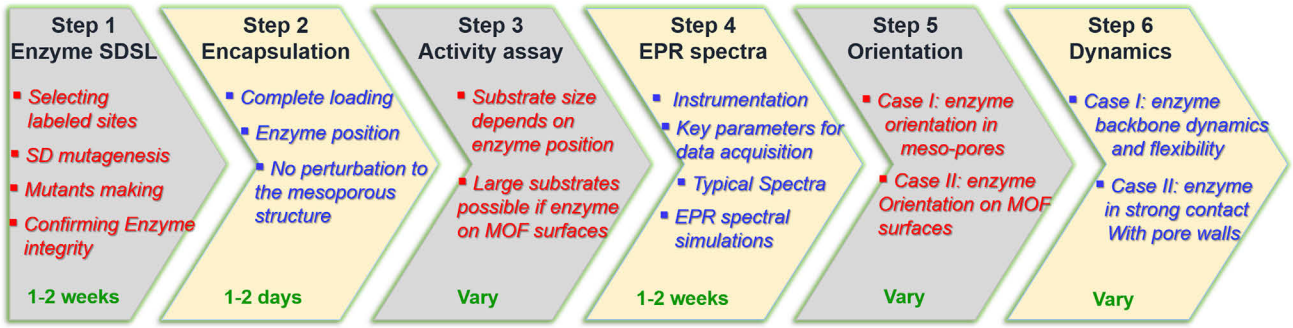

Scheme 1. A general flowchart highlighting the key steps and the timing of each

Six steps are usually taken in order to use SDSL-EPR on enzyme studies upon encapsulation in porous materials. Depending on the purpose of study, certain steps can be skipped or expanded. For details, see the main text.

broadening of CW EPR spectra. The broadening is related to $1/r^6$ and inputs a Pake pattern on top of the regular CW EPR spectra. A simulation program to extract the distance distribution, "ShortDistances" developed by Dr. Altenbach, is available at https://sites.google.com/site/altenbach/labview-programs/epr-programs/short-distances. Note that the measured distances are limited to less than 22 Å; longer than that would result in negligible broadening on the line shape.

In heterogeneous biocatalysis, all the techniques discussed above can certainly be extended to probe enzyme structural information at the interface of enzymes and mesoporous materials. Typical information includes subnanometer- to nanometer-scale enzyme conformational changes upon encapsulation in porous materials and/or contact with binding partners and substrates, as well as the relative orientation of spin centers, which would be related to enzyme function.

In conclusion, we have introduced the principle and general procedures of SDSL-EPR to reveal the relative orientation and residue-level backbone dynamics of enzymes upon encapsulation in mesoporous materials. The goal is to extend the use of this technique to heterogeneous biocatalysis in order to understand the underlying structural basis of enzymes upon encapsulation and eventually help guide the rational design of optimal immobilization platforms. Because of the uniqueness of the technique, at each step of the procedure, we introduced fundamental rules and principles together with typical criteria and parameters requested to optimize the efficiency and accuracy of each step so that interested investigators in biocatalysis or biomaterials science can easily follow them to adapt the technique. In addition, we utilized our own experience as examples to demonstrate our strategies of measuring protein orientation and dynamics and how the structural basis is correlated to the observed catalytic activities. We also offered cautions when carrying out each step in order to avoid pitfalls. Finally, we briefly reviewed the potential of applying alternative EPR spin labels and advanced EPR techniques in revealing enzyme structural basis in biocatalysis in order to broaden the possible application of the EPR technique in understanding enzyme behavior at the molecular level upon encapsulation in various porous materials.

EXPERIMENTAL PROCEDURES

Resource availability

Lead contact

Further information and requests for resources and reagents should be directed to and will be fulfilled by the lead contact, Zhongyu Yang (zhongyu.yang@ndsu.edu).

Materials availability

All unique and stable reagents generated in this study are available from the lead contact without restriction.

Data and code availability

The EPR data supporting the current study have not been deposited in a public repository because of the lack of a proper data resource but are available from the lead contact on request.

SUPPLEMENTAL INFORMATION

Supplemental information can be found online at https://doi.org/10.1016/j.checat.2021.03.005.

ACKNOWLEDGMENTS

This work is supported by the National Science Foundation (MCB 1942596 to Z.Y.), North Dakota State University New Faculty Start-Up Funds, and USDA-NIFA grant 2021-67021-34002 (to B.C.). We appreciate Professor Hubbell for generously providing the EPR spectral simulation package.

AUTHOR CONTRIBUTIONS

Y.P., B.C., and Z.Y. conceived and designed the article. H.L., Q.L., and M.L. assisted in discussions and figure preparation, and X.Z. and B.C. assisted in all analysis and literature search. All authors participated in drafting the manuscript and gave approval to the final version.

DECLARATION OF INTERESTS

The authors declare no competing interests.

Received: February 10, 2021
Revised: March 3, 2021
Accepted: March 12, 2021
Published: April 23, 2021

REFERENCES

1. Nel, A.E., Mädler, L., Velegol, D., Xia, T., Hoek, E.M.V., Somasundaran, P., Klaessig, F., Castranova, V., and Thompson, M. (2009). Understanding biophysicochemical interactions at the nano-bio interface. Nat. Mater. *8*, 543–557.

2. Küchler, A., Yoshimoto, M., Luginbühl, S., Mavelli, F., and Walde, P. (2016). Enzymatic reactions in confined environments. Nat. Nanotechnol. *11*, 409–420.

3. Sheldon, R.A., and Woodley, J.M. (2018). Role of biocatalysis in sustainable chemistry. Chem. Rev. *118*, 801–838.

4. López-Gallego, F., Jackson, E., and Betancor, L. (2017). Heterogeneous systems biocatalysis: the path to the fabrication of self-sufficient artificial metabolic cells. Chem. Euro. J. *23*, 17841–17849.

5. Sheldon, R.A. (2012). Fundamentals of green chemistry: efficiency in reaction design. Chem. Soc. Rev. *41*, 1437–1451.

6. Chapman, R., and Stenzel, M.H. (2019). All wrapped up: stabilization of enzymes within single enzyme nanoparticles. J. Am. Chem. Soc. *141*, 2754–2769.

7. Shemetov, A.A., Nabiev, I., and Sukhanova, A. (2012). Molecular interaction of proteins and peptides with nanoparticles. ACS Nano *6*, 4585–4602.

8. Lee, C.-H., Lin, T.-S., and Mou, C.-Y. (2009). Mesoporous materials for encapsulating enzymes. Nano Today *4*, 165–179.

9. Zhou, Z., and Hartmann, M. (2013). Progress in enzyme immobilization in ordered mesoporous materials and related applications. Chem. Soc. Rev. *42*, 3894–3912.

10. Magner, E. (2013). Immobilisation of enzymes on mesoporous silicate materials. Chem. Soc. Rev. *42*, 6213–6222.

11. Lyu, F., Zhang, Y., Zare, R.N., Ge, J., and Liu, Z. (2014). One-pot synthesis of protein-embedded-supporting information. Nano Lett. *14*, 5761–5765.

12. Wang, X., Lan, P.C., and Ma, S. (2020). Metal-organic frameworks for enzyme immobilization: beyond host matrix materials. ACS Centr. Sci. *6*, 1497–1506.

13. Majewski, M.B., Howarth, A.J., Li, P., Wasielewski, M.R., Hupp, J.T., and Farha, O.K. (2017). Enzyme encapsulation in metal-organic frameworks for applications in catalysis. CrystEngComm *19*, 4082–4091.

14. Drout, R.J., Robison, L., and Farha, O.K. (2019). Catalytic applications of enzymes encapsulated in metal-organic frameworks. Coord. Chem. Rev. *381*, 151–160.

15. Li, P., Chen, Q., Wang, T.C., Vermeulen, N.A., Mehdi, B.L., Dohnalkova, A., Browning, N.D., Shen, D., Anderson, R., Gómez-Gualdrón, D.A., et al. (2018). Hierarchically engineered mesoporous metal-organic frameworks toward cell-free immobilized enzyme systems. Chem *4*, 1022–1034.

16. Li, P., Modica, J.A., Howarth, A.J., Vargas, L.E., Moghadam, P.Z., Snurr, R.Q., Mrksich, M., Hupp, J.T., and Farha, O.K. (2016). Toward

design rules for enzyme immobilization in hierarchical mesoporous metal-organic frameworks. Chem *1*, 154–169.

17. Gkaniatsou, E., Sicard, C.m., Ricoux, R.m., Mahy, J.-P., Steunou, N., and Serre, C. (2017). Metal-organic frameworks: a novel host platform for enzymatic catalysis and detection. Mater. Horiz. *4*, 55–63.

18. Lian, X., Fang, Y., Joseph, E., Wang, Q., Li, J., Banerjee, S., Lollar, C., Wang, X., and Zhou, H.-C. (2017). Enzyme-MOF (metal-organic framework) composites. Chem. Soc. Rev. *46*, 3386–3401.

19. An, H., Song, J., Wang, T., Xiao, N., Zhang, Z., Cheng, P., Huang, H., Ma, S., and Chen, Y. (2020). Metal-organic framework disintegrants: a new generation of enzyme preparation platforms with boosted activity. Angew. Chem. Int. Ed. *59*, 16764–16769.

20. Pan, Y., Li, H., Farmakes, J., Xiao, F., Chen, B., Ma, S., and Yang, Z. (2018). How do enzymes orient on metal-organic framework (MOF) surfaces? J. Am. Chem. Soc. *140*, 16032–16036.

21. Neupane, S., Patnode, K., Li, H., Baryeh, K., Liu, G., Hu, J., Chen, B., Pan, Y., and Yang, Z. (2019). Enhancing enzyme immobilization on carbon nanotubes via metal-organic frameworks for large-substrate biocatalysis. ACS Appl. Mater. Inter. *11*, 12133–12141.

22. Farmakes, J., Schuster, I., Overby, A., Alhalhooly, L., Lenertz, M., Li, Q., Ugrinov, A., Choi, Y., Pan, Y., and Yang, Z. (2020). Enzyme immobilization on graphene oxide (GO) surface via one-pot synthesis of GO/metal-organic framework composites for large-substrate biocatalysis. ACS Appl. Mater. Inter. *12*, 23119–23126.

23. Li, Q., Pan, Y., Li, H., Alhalhooly, L., Li, Y., Chen, B., Choi, Y., and Yang, Z. (2020). Size-tunable metal-organic framework coated magnetic nanoparticles for enzyme encapsulation and large-substrate biocatalysis. ACS Appl. Mater. Interfaces *12*, 41794–41801.

24. Bolivar, J.M., Eisl, I., and Nidetzky, B. (2016). Advanced characterization of immobilized enzymes as heterogeneous biocatalysts. Cataly. Today *259*, 66–80.

25. Zhang, Y., Park, K.-Y., Suazo, K.F., and Distefano, M.D. (2018). Recent progress in enzymatic protein labelling techniques and their applications. Chem. Soc. Rev. *47*, 9106–9136.

26. Janssen, K.P.F., De Cremer, G., Neely, R.K., Kubarev, A.V., Van Loon, J., Martens, J.A., De Vos, D.E., Roeffaers, M.B.J., and Hofkens, J. (2014). Single molecule methods for the study of catalysis: from enzymes to heterogeneous catalysts. Chem. Soc. Rev. *43*, 990–1006.

27. Todd, A.P., Cong, J., Levinthal, F., Levinthal, C., and Hubbell, W.L. (1989). Site-directed mutagenesis of colicin E1 provides specific attachment sites for spin labels whose spectra are sensitive to local conformation. Prot. Struct. Funct. Bioinform. *6*, 294–305.

28. Xiao, H., and Schultz, P.G. (2016). At the interface of chemical and biological synthesis: an expanded genetic code. Cold Spring Harb. Perspect. Biol. *8*, a023945.

29. Kim, C.H., Axup, J.Y., and Schultz, P.G. (2013). Protein conjugation with genetically encoded unnatural amino acids. Curr. Opin. Chem. Biol. *17*, 412–419.

30. Hubbell, W.L., López, C.J., Altenbach, C., and Yang, Z. (2013). Technological advances in site-directed spin labeling of proteins. Curr. Opin. Struct. Biol. *23*, 725–733.

31. Cafiso, D.S. (2014). Identifying and quantitating conformational exchange in membrane proteins using site-directed spin labeling. Acc. Chem. Res. *47*, 3102–3109.

32. McHaourab, H.S., Steed, P.R., and Kazmier, K. (2011). Toward the fourth dimension of membrane protein structure: insight into dynamics from spin-labeling EPR spectroscopy. Structure *19*, 1549–1561.

33. Fanucci, G.E., and Cafiso, D.S. (2006). Recent advances and applications of site-directed spin labeling. Curr. Opin. Struct. Biol. *16*, 644–653.

34. Eaton, S.S., and Eaton, G.R. (1977). Electron paramagnetic resonance sample cell for lossy samples. Anal. Chem. *49*, 1277–1278.

35. Nesmelov, Y.E., Gopinath, A., and Thomas, D.D. (2004). Aqueous sample in an EPR cavity: sensitivity considerations. J. Magn. Reson. *167*, 138–146.

36. Jeschke, G. (2012). DEER distance measurements on proteins. Ann. Rev. Phys. Chem. *63*, 419–446.

37. Borbat, P., and Freed, J. (2014). Pulse dipolar ESR: distance measurements. In Structural Information from Spin-Labels and Intrinsic Paramagnetic Centers in the Biosciences Structure and Bonding, J. Harmer and C. Timmel, eds. (Springer, Heidelberg, Germany), pp. 1–82.

38. Schiemann, O., and Prisner, T.F. (2007). Long-range distance determinations in biomacromolecules by EPR spectroscopy. Quart. Rev. Biophys. *40*, 1–53. https://doi.org/10.1017/S003358350700460X.

39. Martorana, A., Bellapadrona, G., Feintuch, A., Di Gregorio, E., Aime, S., and Goldfarb, D. (2014). Probing protein conformation in cells by EPR distance measurements using Gd3+ spin labeling. J. Am. Chem. Soc. *136*, 13458–13465.

40. Evans, E.G.B., Morgan, J.L.W., DiMaio, F., Zagotta, W.N., and Stoll, S. (2020). Allosteric conformational change of a cyclic nucleotide-gated ion channel revealed by DEER spectroscopy. Proc. Natl. Acad. Sci. USA *117*, 10839–10847.

41. Puljung, M.C., DeBerg, H.A., Zagotta, W.N., and Stoll, S. (2014). Double electron-electron resonance reveals cAMP-induced conformational change in HCN channels. Proc. Natl. Acad. Sci. USA *111*, 9816.

42. Hubbell, W.L., Gross, A., Langen, R., and Lietzow, M.A. (1998). Recent advances in site-directed spin labeling of proteins. Curr. Opin. Struct. Biol. *8*, 649–656.

43. Van Eps, N., Thomas, C.J., Hubbell, W.L., and Sprang, S.R. (2015). The guanine nucleotide exchange factor Ric-8A induces domain separation and Ras domain plasticity in G伪i1. Proc. Natl. Acad. Sci. USA *112*, 1404–1409.

44. Yang, Z., Kurpiewski, M.R., Ji, M., Townsend, J.E., Mehta, P., Jen-Jacobson, L., and Saxena, S. (2012). ESR spectroscopy identifies inhibitory Cu2+ sites in a DNA-modifying enzyme to reveal determinants of catalytic specificity. Proc. Natl. Acad. Sci. USA *109*, E993–E1000.

45. Zou, P., Bortolus, M., and McHaourab, H.S. (2009). Conformational cycle of the ABC transporter MsbA in liposomes: detailed analysis using double electron-electron resonance spectroscopy. J. Mol. Biol. *393*, 586–597.

46. Singewald, K., Lawless, M.J., and Saxena, S. (2019). Increasing nitroxide lifetime in cells to enable in-cell protein structure and dynamics measurements by electron spin resonance spectroscopy. J. Magn. Reson. *299*, 21–27.

47. Karthikeyan, G., Bonucci, A., Casano, G., Gerbaud, G., Abel, S.b., ThomÃ©, V., Kodjabachian, L., Magalon, A., Guigliarelli, B., Belle, V.r., et al. (2018). A bioresistant nitroxide spin label for in-cell EPR spectroscopy: in vitro and in oocytes protein structural dynamics studies. Angew. Chem. Int. Ed. *57*, 1366–1370.

48. Krstić, I., Hänsel, R., Romainczyk, O., Engels, J.W., Dötsch, V., and Prisner, T.F. (2011). Long-range distance measurements on nucleic acids in cells by pulsed EPR spectroscopy. Angew. Chem. Int. Ed. *50*, 5070–5074.

49. Bode, B.E., Margraf, D., Plackmeyer, J., Dürner, G., Prisner, T.F., and Schiemann, O. (2007). Counting the monomers in nanometer-sized oligomers by pulsed electron-electron double resonance. J. Am. Chem. Soc. *129*, 6736–6745.

50. Endeward, B., Butterwick, J.A., MacKinnon, R., and Prisner, T.F. (2009). Pulsed electron-electron double-resonance determination of spin-label distances and orientations on the tetrameric potassium ion channel KcsA. J. Am. Chem. Soc. *131*, 15246–15250.

51. Zhang, X., Tung, C.-S., Sowa, G.Z., Hatmal, M.m.M., Haworth, I.S., and Qin, P.Z. (2012). Global structure of a three-way junction in a Phi29 packaging RNA dimer determined using site-directed spin labeling. J. Am. Chem. Soc. *134*, 2644–2652.

52. Joseph, B., Jeschke, G., Goetz, B.A., Locher, K.P., and Bordignon, E. (2011). Transmembrane gate movements in the type II ATP-binding cassette (ABC) importer BtuCD-F during nucleotide cycle. J. Biol. Chem. *286*, 41008–41017.

53. Bordignon, E., Seeger, M.A., Galazzo, L., and Meier, G. (2020). From in vitro towards in situ: structure-based investigation of ABC exporters by electron paramagnetic resonance spectroscopy. FEBS Lett. *594*, 3839–3856.

54. Galazzo, L., Meier, G., Timachi, M.H., Hutter, C.A.J., Seeger, M.A., and Bordignon, E. (2020). Spin-labeled nanobodies as protein conformational reporters for electron paramagnetic resonance in cellular

membranes. Proc. Natl. Acad. Sci. USA *117*, 2441.

55. Hutter, C.A.J., Timachi, M.H., Hürlimann, L.M., Zimmermann, I., Egloff, P., Göddeke, H., Kucher, S., Štefanić, S., Karttunen, M., Schäfer, L.V., et al. (2019). The extracellular gate shapes the energy profile of an ABC exporter. Nat. Commun. *10*, 2260.

56. Fleck, N., Heubach, C.A., Hett, T., Haege, F.R., Bawol, P.P., Baltruschat, H., and Schiemann, O. (2020). SLIM: a short-linked, highly redox-stable trityl label for high-sensitivity in-cell EPR distance measurements. Angew. Chem. Int. Ed. *59*, 9767–9772.

57. Jassoy, J.J., Berndhäuser, A., Duthie, F., Kühn, S.P., Hagelueken, G., and Schiemann, O. (2017). Versatile trityl spin labels for nanometer distance measurements on biomolecules in vitro and within cells. Angew. Chem. Int. Ed. *56*, 177–181.

58. Joseph, B., Sikora, A., Bordignon, E., Jeschke, G., Cafiso, D.S., and Prisner, T.F. (2015). Distance measurement on an endogenous membrane transporter in *E. coli* cells and native membranes using EPR spectroscopy. Angew. Chem. Int. Ed. *54*, 6196–6199.

59. Abdullin, D., Florin, N., Hagelueken, G., and Schiemann, O. (2015). EPR-based approach for the localization of paramagnetic metal ions in biomolecules. Angew. Chem. *54*, 1827–1831.

60. Karthikeyan, G., Bonucci, A., Casano, G., Gerbaud, G., Abel, S., Thomé, V., Kodjabachian, L., Magalon, A., Guigliarelli, B., Belle, V., et al. (2018). A bioresistant nitroxide spin label for in-cell EPR spectroscopy: in vitro and in oocytes protein structural dynamics studies. Angew. Chem. Int. Ed. *57*, 1366–1370.

61. Pan, Y., Li, Q., Li, H., Farmakes, J., Ugrinov, A., Zhu, X., et al. (2021). A general Ca-MOM platform with enhanced acid-base stability for enzyme biocatalysis. Chem. Catal. *1*, https://doi.org/10.1016/j.checat.2021.03.001.

62. Sun, Q., Pan, Y., Wang, X., Li, H., Farmakes, J., Aguila, B., Yang, Z., and Ma, S. (2019). Mapping out the degree of freedom of hosted enzymes in confined spatial environments. Chem *5*, 3184–3195.

63. Hyde, J.S., Yin, J.-J., Froncisz, W., and Feix, J.B. (1985). Electron-electron double resonance (ELDOR) with a loop-gap resonator. J. Magn. Reson. (1969) *63*, 142–150.

64. Froncisz, W., and Hyde, J.S. (1982). The loop-gap resonator: a new microwave lumped circuit ESR sample structure. J. Magn. Reson. (1969) *47*, 515–521.

65. Goldfarb, D. (2014). Gd3+ spin labeling for distance measurements by pulse EPR spectroscopy. Phys. Chem. Chem. Phys. *16*, 9685–9699.

66. Singewald, K., Bogetti, X., Sinha, K., Rule, G.S., and Saxena, S. (2020). Double histidine based EPR measurements at physiological temperatures permit site-specific elucidation of hidden dynamics in enzymes. Angew. Chem. Int. Ed. *59*, 23040–23044.

67. Yulikov, M., Lueders, P., Farooq Warsi, M., Chechik, V., and Jeschke, G. (2012). Distance measurements in Au nanoparticles functionalized with nitroxide radicals and Gd3+-DTPA chelate complexes. Phys. Chem. Chem. Phys. *14*, 10732–10746.

68. Budil, D.E., Lee, S., Saxena, S., and Freed, J.H. (1996). Nonlinear-least-squares analysis of slow-motion EPR spectra in one and two dimensions using a modified Levenberg-Marquardt algorithm. J. Magn. Reson. A. *120*, 155–189.

69. Altenbach, C., López, C.J., Hideg, K., Hubbell, W.L., Peter, Z.Q., and Kurt, W. (2015). Chapter three - exploring structure, dynamics, and topology of nitroxide spin-labeled proteins using continuous-wave electron paramagnetic resonance spectroscopy. In Methods in Enzymology (Academic Press), pp. 59–100.

70. López, C.J., Fleissner, M.R., Guo, Z., Kusnetzow, A.K., and Hubbell, W.L. (2009). Osmolyte perturbation reveals conformational equilibria in spin-labeled proteins. Prot. Sci. *18*, 1637–1652.

71. Fleissner, M.R., Bridges, M.D., Brooks, E.K., Cascio, D., Kálai, T., Hideg, K., and Hubbell, W.L. (2011). Structure and dynamics of a conformationally constrained nitroxide side chain and applications in EPR spectroscopy. Proc. Natl. Acad. Sci. USA *108*, 16241–16246.

72. Zhang, Z., Fleissner, M.R., Tipikin, D.S., Liang, Z., Moscicki, J.K., Earle, K.A., Hubbell, W.L., and Freed, J.H. (2010). Multifrequency electron spin resonance study of the dynamics of spin labeled T4 lysozyme. J. Phys. Chem. B *114*, 5503–5521.

73. Steinhoff, H.J. (2005). Multi-frequency EPR spectroscopy studies of the structure and conformational changes of site-directed spin labelled membrane proteins. In Supramolecular Structure and Function 8, G. Pifat-Mrzljak, ed. (Springer), pp. 157–177.

74. Borovykh, I.V., Ceola, S., Gajula, P., Gast, P., Steinhoff, H.-J., and Huber, M. (2006). Distance between a native cofactor and a spin label in the reaction centre of Rhodobacter sphaeroides by a two-frequency pulsed electron paramagnetic resonance method and molecular dynamics simulations. J. Magn. Reson. *180*, 178–185.

75. Möbius, K. (2009). Chapter 5 applications of high-field EPR on selected proteins and their model systems. In High-Field EPR Spectroscopy on Proteins and Their Model Systems: Characterization of Transient Paramagnetic States (The Royal Society of Chemistry)), pp. 206–350.

76. Columbus, L., Kálai, T., Jekö, J., Hideg, K., and Hubbell, W.L. (2001). Molecular motion of spin labeled side chains in α-helices: analysis by variation of side chain structure. Biochemistry *40*, 3828–3846.

77. Columbus, L., and Hubbell, W.L. (2004). Mapping backbone dynamics in solution with site-directed spin labeling: GCN4-58 bZip free and bound to DNA. Biochemistry *43*, 7273–7287.

78. Lyubenova, S., Maly, T., Zwicker, K., Brandt, U., Ludwig, B., and Prisner, T. (2009). Multifrequency pulsed electron paramagnetic resonance on metalloproteins. Acc. Chem. Res. *43*, 181–189.

79. Stoll, S., and Schweiger, A. (2006). EasySpin, a comprehensive software package for spectral simulation and analysis in EPR. J. Magn. Reson. *178*, 42–55.

80. Pan, Y., Neupane, S., Farmakes, J., Bridges, M., Froberg, J., Rao, J., Qian, S.Y., Liu, G., Choi, Y., and Yang, Z. (2017). Probing the structural basis and adsorption mechanism of an enzyme on nano-sized protein carriers. Nanoscale *9*, 3512–3523.

81. Kroncke, B.M., Horanyi, P.S., and Columbus, L. (2010). Structural origins of nitroxide side chain dynamics on membrane protein a-helical sites. Biochemistry *49*, 10045–10060.

82. Oldham, W.M., Van Eps, N., Preininger, A.M., Hubbell, W.L., and Hamm, H.E. (2007). Mapping allosteric connections from the receptor to the nucleotide-binding pocket of heterotrimeric G proteins. Proc. Natl. Acad. Sci. USA *104*, 7927–7932.

83. Margittai, M., and Langen, R. (2004). Template-assisted filament growth by parallel stacking of tau. Proc. Natl. Acad. Sci. USA *101*, 10278–10283.

84. Chen, M., Margittai, M., Chen, J., and Langen, R. (2007). Investigation of α-synuclein fibril structure by site-directed spin labeling. J. Biol. Chem. *282*, 24970–24979.

85. Bordignon, E. (2017). EPR spectroscopy of nitroxide spin probes (eMagRes), pp. 235–254.

86. Sahu, I.D., and Lorigan, G.A. (2018). Site-directed spin labeling EPR for studying membrane proteins. Biomed. Res. Inter. *2018*. 3248289. https://doi.org/10.1155/2018/3248289.

87. Yang, Z., Jiménez-Osés, G., López, C.J., Bridges, M.D., Houk, K.N., and Hubbell, W.L. (2014). Long-range distance measurements in proteins at physiological temperatures using saturation recovery EPR spectroscopy. J. Am. Chem. Soc. *136*, 15356–15365.

88. Stoller, S., Sicoli, G., Baranova, T.Y., Bennati, M., and Diederichsen, U. (2011). TOPP: a novel nitroxide-labeled amino acid for EPR distance measurements. Angew. Chem. Int. Ed. *50*, 9743–9746.

89. Yang, Z., Liu, Y., Borbat, P., Zweier, J.L., Freed, J.H., and Hubbell, W.L. (2012). Pulsed ESR dipolar spectroscopy for distance measurements in immobilized spin labeled proteins in liquid solution. J. Am. Chem. Soc. *134*, 9950–9952.

90. Reginsson, G.W., Kunjir, N.C., Sigurdsson, S.T., and Schiemann, O. (2012). Trityl radicals: spin labels for nanometer-distance measurements. Chem. Euro. J. *18*, 13580–13584.

91. Kunjir, N.C., Reginsson, G.W., Schiemann, O., and Sigurdsson, S.T. (2013). Measurements of short distances between trityl spin labels with CW EPR, DQC and PELDOR. Phys. Chem. Chem. Phys. *15*, 19673–19685.

92. Shevelev, G.Y., Krumkacheva, O.A., Lomzov, A.A., Kuzhelev, A.A., Rogozhnikova, O.Y., Trukhin, D.V., Troitskaya, T.I., Tormyshev, V.M., Fedin, M.V., Pyshnyi, D.V., et al. (2014). Physiological-temperature distance measurement in nucleic acid using

triarylmethyl-based spin labels and pulsed dipolar EPR spectroscopy. J. Am. Chem. Soc. *136*, 9874–9877.

93. Kuzhelev, A.A., Trukhin, D.V., Krumkacheva, O.A., Strizhakov, R.K., Rogozhnikova, O.Y., Troitskaya, T.I., Fedin, M.V., Tormyshev, V.M., and Bagryanskaya, E.G. (2015). Room-temperature electron spin relaxation of triarylmethyl radicals at the X- and Q-bands. J. Phys. Chem. B *119*, 13630–13640.

94. Potapov, A., Yagi, H., Huber, T., Jergic, S., Dixon, N.E., Otting, G., and Goldfarb, D. (2010). Nanometer-scale distance measurements in proteins using Gd3+ spin labeling. J. Am. Chem. Soc. *132*, 9040–9048.

95. Lueders, P., Jeschke, G., and Yulikov, M. (2011). Double electron-electron resonance measured between Gd3+ ions and nitroxide radicals. J. Phys. Chem. Lett. *2*, 604–609.

96. Garbuio, L., Bordignon, E., Brooks, E.K., Hubbell, W.L., Jeschke, G., and Yulikov, M. (2013). Orthogonal spin labeling and Gd(III)-nitroxide distance measurements on bacteriophage T4-lysozyme. J. Phys. Chem. B *117*, 3145–3153.

97. Matalon, E., Huber, T., Hagelueken, G., Graham, B., Frydman, V., Feintuch, A., Otting, G., and Goldfarb, D. (2013). Gadolinium(III) spin labels for high-sensitivity distance measurements in transmembrane helices. Angew. Chem. Int. Ed. *52*, 11831–11834.

98. Fleissner, M.R., Brustad, E.M., Kálai, T., Altenbach, C., Cascio, D., Peters, F.B., Hideg, K., Peuker, S., Schultz, P.G., and Hubbell, W.L. (2009). Site-directed spin labeling of a genetically encoded unnatural amino acid. Proc. Natl. Acad. Sci. USA *106*, 21637–21642.

99. López, C.J., Fleissner, M.R., Brooks, E.K., and Hubbell, W.L. (2014). Stationary-phase EPR for exploring protein structure, conformation, and dynamics in spin-labeled proteins. Biochemistry *53*, 7067–7075.

100. Ji, M., Ruthstein, S., and Saxena, S. (2014). Paramagnetic metal ions in pulsed ESR distance distribution measurements. Acc. Chem. Res. *47*, 688–695.

101. Cunningham, T.F., Putterman, M.R., Desai, A., Horne, W.S., and Saxena, S. (2015). The double-histidine Cu2+-binding motif: a highly rigid, site-specific spin probe for electron spin resonance distance measurements. Angew. Chem. Int. Ed. *54*, 6330–6334.

102. Gamble Jarvi, A., Bogetti, X., Singewald, K., Ghosh, S., and Saxena, S. (2021). Going the dHis-tance: site-directed Cu2+ labeling of proteins and nucleic acids. Acc. Chem. Res. https://doi.org/10.1021/acs.accounts.0c00761.

103. Akhmetzyanov, D., Plackmeyer, J., Endeward, B., Denysenkov, V., and Prisner, T.F. (2015). Pulsed electron-electron double resonance spectroscopy between a high-spin Mn2+ ion and a nitroxide spin label. Phys. Chem. Chem. Phys. *17*, 6760–6766.

104. Kaminker, I., Bye, M., Mendelman, N., Gislason, K., Sigurdsson, S.T., and Goldfarb, D. (2015). Distance measurements between manganese(ii) and nitroxide spin-labels by DEER determine a binding site of Mn2+ in the HP92 loop of ribosomal RNA. Phys. Chem. Chem. Phys. *17*, 15098–15102.

105. Banerjee, D., Yagi, H., Huber, T., Otting, G., and Goldfarb, D. (2012). Nanometer-range distance measurement in a protein using Mn2+ tags. J. Phys. Chem. Lett. *3*, 157–160.

106. Jeschke, G., Chechik, V., Ionita, P., Godt, A., Zimmermann, H., Banham, J., Timmel, C.R., Hilger, D., and Jung, H. (2006). DeerAnalysis2006—a comprehensive software package for analyzing pulsed ELDOR data. Appl. Magn. Reson. *30*, 473–498.

107. Marko, A., and Prisner, T.F. (2013). An algorithm to analyze PELDOR data of rigid spin label pairs. Phys. Chem. Chem. Phys. *15*, 619–627.

108. Marko, A., Margraf, D., Yu, H., Mu, Y., Stock, G., and Prisner, T. (2009). Molecular orientation studies by pulsed electron-electron double resonance experiments. J. Chem. Phys. *130*, 064102.

109. Bode, B.E., Plackmeyer, J., Prisner, T.F., and Schiemann, O. (2008). PELDOR measurements on a nitroxide-labeled Cu(II) porphyrin: orientation selection, spin-density distribution, and conformational flexibility. J. Phys. Chem. A *112*, 5064–5073.

110. Denysenkov, V.P., Prisner, T.F., Stubbe, J., and Bennati, M. (2006). High-field pulsed electron-electron double resonance spectroscopy to determine the orientation of the tyrosyl radicals in ribonucleotide reductase. Proc. Natl. Acad. Sci. USA *103*, 13386–13390.

111. Abdullin, D., Hagelueken, G., Hunter, R.I., Smith, G.M., and Schiemann, O. (2015). Geometric model-based fitting algorithm for orientation-selective PELDOR DATA. Mol. Phys. *113*, 544–560.

112. Kaminker, I., Florent, M., Epel, B., and Goldfarb, D. (2011). Simultaneous acquisition of pulse EPR orientation selective spectra. J. Magn. Reson. *208*, 95–102.

113. Lovett, J.E., Bowen, A.M., Timmel, C.R., Jones, M.W., Dilworth, J.R., Caprotti, D., Bell, S.G., Wong, L.L., and Harmer, J. (2009). Structural information from orientationally selective DEER spectroscopy. Phys. Chem. Chem. Phys. *11*, 6840–6848.

114. Reginsson, G.W., Hunter, R.I., Cruickshank, P.A.S., Bolton, D.R., Sigurdsson, S.T., Smith, G.M., and Schiemann, O. (2012). W-band PELDOR with 1 kW microwave power: molecular geometry, flexibility and exchange coupling. J. Magn. Reson. *216*, 175–182.

115. Keller, K., Ritsch, I., Hintz, H., Hülsmann, M., Qi, M., Breitgoff, F.D., Klose, D., Polyhach, Y., Yulikov, M., Godt, A., et al. (2020). Accessing distributions of exchange and dipolar couplings in stiff molecular rulers with Cu(ii) centres. Phys. Chem. Chem. Phys. *22*, 21707–21730.

116. Weber, A., Schiemann, O., Bode, B., and Prisner, T.F. (2002). PELDOR at S- and X-band frequencies and the separation of exchange coupling from dipolar coupling. J. Magn. Reson. *157*, 277–285.

117. Margraf, D., Cekan, P., Prisner, T.F., Sigurdsson, S.T., and Schiemann, O. (2009). Ferro- and antiferromagnetic exchange coupling constants in PELDOR spectra. Phys. Chem. Chem. Phys. *11*, 6708–6714.

118. Bode, B.E., Plackmeyer, J., Bolte, M., Prisner, T.F., and Schiemann, O. (2009). PELDOR on an exchange coupled nitroxide copper(II) spin pair. J. Organometal. Chem. *694*, 1172–1179.

119. Borbat, P.P., Freed, J.H., Melvin, I., Simon, B.R.C., and Alexandrine, C. (2007). Measuring distances by pulsed dipolar ESR spectroscopy: spin-labeled histidine Kinases. Methods in Enzymology (Academic Press), pp. 52–116.

120. Saxena, S., and Freed, J.H. (1997). Theory of double quantum two-dimensional electron spin resonance with application to distance measurements. J. Chem. Phys. *107*, 1317–1340.

121. Bridges, M., Hideg, K., and Hubbell, W. (2010). Resolving conformational and rotameric exchange in spin-labeled proteins using saturation recovery EPR. Appl. Magn. Reson. *37*, 363–390.

122. Yang, Z., Bridges, M., Lopez, C., Rogozhnikova, O.Y., Trukhin, D., Brooks, E., Tormyshev, V., Halpern, H., and Hubbell, W. (2016). A triarylmethyl spin label for long-range distance measurement at physiological temperature using T1 relaxation enhancement. J. Magn. Reson. *269*, 50–54.

123. Lyubenova, S., Siddiqui, M.K., Penning de Vries, M.J.M., Ludwig, B., and Prisner, T.F. (2007). Protein-protein interactions studied by EPR relaxation measurements: cytochrome c and cytochrome c oxidase. J. Phys. Chem. B *111*, 3839–3846.

124. Jäger, H., Koch, A., Maus, V., Spiess, H.W., and Jeschke, G. (2008). Relaxation-based distance measurements between a nitroxide and a lanthanide spin label. J. Magn. Reson. *194*, 254–263.

125. Sarver, J., Silva, K.I., and Saxena, S. (2013). Measuring Cu2+-nitroxide distances using double electron-electron resonance and saturation recovery. Appl. Magn. Reson. *44*, 583–594.

126. Lueders, P., Jäger, H., Hemminga, M.A., Jeschke, G., and Yulikov, M. (2012). Multiple pathway relaxation enhancement in the system composed of three paramagnetic species: nitroxide radical-Ln^{3+}-O_2. J. Phys. Chem. Lett. *3*, 1336–1340.

127. Razzaghi, S., Brooks, E.K., Bordignon, E., Hubbell, W.L., Yulikov, M., and Jeschke, G. (2013). EPR relaxation-enhancement-based distance measurements on orthogonally spin-labeled T4-lysozyme. ChemBioChem *14*, 1883–1890.

128. Altenbach, C., Oh, K.-J., Trabanino, R.J., Hideg, K., and Hubbell, W.L. (2001). Estimation of inter-residue distances in spin labeled proteins at physiological temperatures: experimental strategies and practical limitations. Biochemistry *40*, 15471–15482.